https://doi.org/10.5194/acp-2020-1296
Preprint. Discussion started: 7 January 2021

Atmospheric Chemistry and Physics
Discussions
Open Access
EGU

Present and future aerosol impacts on Arctic climate change in the GISS-E2.1 Earth system model

Ulas Im[1,2,*], Kostas Tsigaridis[3,4], Gregory Faluvegi[3,4], Peter L. Langen[1,2], Joshua P. French[5], Rashed Mahmood[6], Thomas Manu[7], Knut von Salzen[8], Daniel C. Thomas[1,2], Cynthia H. Whaley[8], Zbigniew Klimont[9], Henrik Skov[1,2], Jørgen Brandt[1,2]

[1]Department of Environmental Science, Aarhus University, Roskilde, Denmark.
[2] Interdisciplinary Centre for Climate Change, Aarhus University, Roskilde, Denmark.
[3] Center for Climate Systems Research, Columbia University, New York, NY, USA.
[4] NASA Goddard Institute for Space Studies, New York, NY, USA.
[5] Department of Mathematical and Statistical Sciences, University of Colorado Denver, USA.
[6] Barcelona Supercomputing Center, Barcelona, Spain.
[7] Swedish Meteorological and Hydrological Institute, Norrköping, Sweden.
[8] Candian Centre for Climate Modelling and Analysis, Environment and Climate Change Canada, Victoria, British Columbia, Canada.
[9] International Institute for Applied Systems Analysis (IIASA), Laxenburg, Austria.
[*] Corresponding author

Abstract

The Arctic is warming two to three times faster than the global average, partly due to changes in short-lived climate forcers (SLCFs) including aerosols. In order to study the effects of atmospheric aerosols in this warming, recent past (1990-2014) and future (2015-2050) simulations have been carried out using the GISS-E2.1 Earth system model to study the aerosol burdens and their radiative and climate impacts over the Arctic (>60 °N), using anthropogenic emissions from the Eclipse V6b and the Coupled Model Intercomparison Project Phase 6 (CMIP6) databases.

Surface aerosol levels, in particular black carbon (BC) and sulfate (SO_4^{2-}), have been significantly underestimated by more than 50%, with the smallest biases calculated for the nudged atmosphere-only simulations. CMIP6 simulations performed slightly better in simulating both surface concentrations of aerosols and climate parameters, compared to the Eclipse simulations. In addition, fully-coupled simulations had slightly smaller biases in aerosol levels compared to atmosphere only simulations without nudging.

Arctic BC, organic carbon (OC) and SO_4^{2-} burdens decrease significantly in all simulations following the emission projections, with the CMIP6 ensemble showing larger reductions in Arctic aerosol burdens compared to the Eclipse ensemble. For the 2030-2050 period, both the Eclipse Current Legislation (CLE) and the Maximum Feasible Reduction (MFR) ensembles simulated an aerosol top of the atmosphere (TOA) forcing of -0.39±0.01 W m^{-2}, of which -0.24±0.01 W m^{-2} were attributed to the anthropogenic aerosols. The CMIP6 SSP3-7.0 scenario simulated a TOA aerosol forcing of -0.35 W m^{-2} for the same period, while SSP1-2.6 and SSP2-4.5 scenarios simulated a slightly more negative TOA forcing (-0.40 W m^{-2}), of which the anthropogenic aerosols accounted for -0.26 W m^{-2}. Finally, all simulations showed

an increase in the Arctic surface air temperatures both throughout the simulation period. In 2050, surface air temperatures are projected to increase by 2.4 °C to 2.6 °C in the Eclipse ensemble and 1.9 °C to 2.6 °C in the CMIP6 ensemble, compared to the 1990-2010 mean.

Overall, results show that even the scenarios with largest emission reductions lead to similar impact on the future Arctic surface air temperatures compared to scenarios with smaller emission reductions, while scenarios no or little mitigation leads to much larger sea-ice loss, implying that even though the magnitude of aerosol reductions lead to similar responses in surface air temperatures, high mitigation of aerosols are still necessary to limit sea-ice loss.

1. Introduction

The Arctic is warming two to three times faster than the global average (IPCC, 2013; Lenssen et al., 2019). This is partly due to internal Arctic feedback mechanisms, such as the snow and sea-ice-albedo feedback, where melting ice leads to increased absorption of solar radiation, which further enhances warming in the Arctic (Serreze and Francis, 2006). However, Arctic temperatures are also affected by interactions with warming at lower latitudes (e.g., Stuecker et al., 2018; Graversen and Langen, 2019; Semmler et al., 2020) and by local in situ response to radiative forcing due to changes in greenhouse gases and aerosols in the area (Shindell, 2007; Stuecker et al., 2018). In addition to warming induced by increases in global atmospheric carbon dioxide (CO_2) concentrations, changes in short-lived climate forcers (SLCFs) such as tropospheric ozone (O_3), methane (CH_4) and aerosols (e.g. black carbon (BC) and sulfate (SO_4^{2-})) in the Northern Hemisphere (NH), have contributed substantially to the Arctic warming since 1890 (Shindell and Faluvegi, 2009; Ren et al., 2020). This contribution from SLCFs to Arctic heating together with efficient local amplification mechanisms put a high priority on understanding the sources and sinks of SLCFs at high latitudes and their corresponding climatic effects.

SLCFs include all atmospheric species, which have short residence times in the atmosphere relative to long-lived greenhouse gases and have the potential to affect Earth's radiative energy budget. Aerosols are important SLCFs and are a predominant component of air quality that affects human health (Burnett et al., 2018, Lelieveld et al., 2019). They mostly affect climate by altering the amount of solar energy absorbed by Earth and are efficiently removed from the troposphere within several days to weeks. Black carbon (BC), which is a product of incomplete combustion and open biomass/biofuel burning (Bond et al., 2004: 2013), absorbs a high proportion of incident solar radiation and therefore warms the climate system (Jacobson, 2001). Sulphate (SO_4^{2-}), which is formed primarily through oxidation of sulphur dioxide (SO_2), absorbs negligible solar radiation and cools climate by scattering solar radiation back to space. Organic carbon (OC), which is co-emitted with BC during combustion, both scatters and absorbs solar radiation and therefore causes cooling in some environments and warming in others. Highly reflective regions such as the Arctic are more likely to experience warming effects from these aerosols (e.g., Myhre et al, 2013).

https://doi.org/10.5194/acp-2020-1296
Preprint. Discussion started: 7 January 2021

Aerosols also influence climate via indirect mechanisms. After depositing onto snow and ice surfaces, BC can amplify ice melt by lowering the albedo and increasing solar heating of the surface (AMAP, 2015). Aerosols also affect cloud properties, including their droplet size, lifetime, and vertical extent, thereby influencing both the shortwave cooling and longwave warming effects of clouds. Globally, this indirect cloud forcing from aerosols is likely larger than their direct forcing, although the indirect effects are more uncertain and difficult to accurately quantify (IPCC, 2013). Moreover, Arctic cloud impacts are distinct from global impacts, owing to the extreme seasonality of solar radiation in the Arctic, unique characteristics of Arctic clouds (e.g., high frequency of mixed-phase occurrence), and rapidly evolving sea-ice distributions. Together, they lead to complicated and unique phenomena that govern Arctic aerosol abundances and climate impacts (e.g., Willis et al., 2018; Abbatt et al., 2019). The changes taking place in the Arctic have consequences for how SLCFs affect the region. For example, reductions in sea-ice extent, thawing of permafrost, and humidification of the Arctic troposphere can affect the emissions, lifetime and radiative forcing of SLCFs within the Arctic (Thomas et al., 2019).

The effect of aerosols on the Arctic climate through the effects of scattering and absorption of radiation, clouds, and surface ice/snow albedo has been investigated in previous studies (i.e. Clarke and Noone, 1985; Flanner et al., 2007; Shindell et al., 2012; Bond et al., 2013; Dumont et al., 2014). Arctic climate change through aerosols is mainly driven by a response to remote forcings (Gagné et al., 2015; Sand et al., 2015; Westervelt et al., 2015). Lewinschal et al. (2019) estimated an Arctic temperature change per unit sulfur emission of -0.020 to -0.025 K per TgS yr^{-1}. Sand et al. (2020) calculated an Arctic surface air temperature response of 0.06 - 0.1 K per Tg BC yr^{-1} to BC emissions in Europe and North America, and slightly lower response (0.05-0.08 K per Tg BC yr^{-1}) to Asian emissions. Breider et al. (2017) reported a short-wave (SW) aerosol radiative forcing (ARF) of −0.19 ± 0.05 W m^{-2} at the top of the atmosphere (TOA) over the Arctic, which reflects the balance between sulphate cooling (−0.60 W m^{-2}) and black carbon (BC) warming (+0.44 W m^{-2}). Schacht et al. (2019) calculated a direct radiative forcing of up to 0.4 W m^{-2} over the Arctic using the ECHAM6.3-HAM2.3 global aerosol-climate model. Markowicz et al. (2021), using the NAAPS radiative transfer model, calculated the total aerosol forcing over the Arctic (>70.5 °N) of -0.4 W m^{-2}. Ren et al. (2020) simulated 0.11 and 0.25 W m^{-2} direct and indirect warning in 2014-2018 compared to 1980-1984 due to reductions in sulfate, using the CAM5-EAST global aerosol-climate model. They also reported that the aerosols produced an Arctic surface warming of +0.30 °C during 1980–2018, explaining about 20% of the observed Arctic warming observed during the last four decades, while according to Shindell and Faluvegi (2009), aerosols contributed 1.09 ± 0.81 °C to the observed Arctic surface air temperature increase of 1.48 ± 0.28 °C observed in 1976-2007. AMAP (2015), based on four ESMs, estimated a total Arctic surface air temperature response due to the direct effect of current global combustion derived BC, OC and sulfur emissions to be +0.35 °C, of which +0.40 °C was attributed to BC in the atmosphere, +0.22 °C to BC in snow, -0.04 °C to OC and -0.23 °C to SO_4^{2-}. Samset et al. (2018) showed that Arctic warming due to aerosol reductions can reach up to 4°C in some locations, with a multi-model increase for the 60°N–90°N region being 2.8°C. In addition, recent studies also suggest that as global emissions of anthropogenic aerosols decrease,

https://doi.org/10.5194/acp-2020-1296
Preprint. Discussion started: 7 January 2021

natural aerosol feedbacks may become increasingly important for Arctic climate (Boy et al., 2019; Mahmood et al., 2019).

In this study, we carry out several simulations with the fully coupled NASA Goddard Institute of Space Sciences (GISS) earth system model, GISS-E2.1 (Kelley et al., 2020) to study the recent past and future burdens of aerosols as well as their impacts on TOA radiative forcing and climate-relevant parameters such as surface air temperatures, sea-ice, and snow over the Arctic (>60 °N). In addition, we investigate the impacts from two different emission inventories; Eclipse V6b (Höglund-Isaksson et al.,2020; Klimont et al., 2021) vs. CMIP6 (Hoesly et al., 2018; van Marle et al., 2017: Feng et al.,2020), as well as differences between atmosphere-only vs. fully-coupled simulations, on the evaluation of the model and the climate impact. Section 2 introduces the GISS-E2.1 model, the anthropogenic emissions, and the observation datasets used in model evaluation. Section 3 presents results from the model evaluation as well as recent past and future trends in simulated aerosol burdens, radiative forcing, and climate change over the Arctic. Section 4 summarizes the overall findings and the conclusions.

2. Materials and methods

2.1. Model description

GISS-E2.1 is the CMIP6 version of the GISS modelE Earth system model, which has been validated extensively over the globe (Kelly et al., 2020; Bauer et al., 2020) as well as regionally for air pollutants (Turnock et al., 2020). A full description of GISS-E2.1 and evaluation of its coupled climatology during the satellite era (1979–2014) and the recent past ensemble simulation of the atmosphere and ocean component models (1850-2014) are described in Kelly et al. (2020) and Miller et al. (2020), respectively. GISS-E2.1 has a horizontal resolution of 2° in latitude by 2.5° in longitude and 40 vertical layers extending from the surface to 0.1 hPa in the lower mesosphere. The tropospheric chemistry scheme used in GISS-E2.1 (Shindell et al., 2013) includes inorganic chemistry of O_x, NO_x, HO_x, CO, and organic chemistry of CH_4 and higher hydrocarbons using the CBM4 scheme (Gery et al., 1989), and the stratospheric chemistry scheme (Shindell et al., 2013), which includes chlorine and bromine chemistry together with polar stratospheric clouds.

In the present work, we used the One-Moment Aerosol scheme (OMA: Bauer et al., 2020 and references therein), which is a mass-based scheme in which aerosols are assumed to remain externally mixed and have a prescribed and constant size distribution, with the exception of sea salt that has two distinct size classes, and dust that is described by a sectional model with an option from 4 to 6 bins. The default dust configuration that is used in this work includes 5 bins, a clay and 4 silt ones, from submicron to 16 µm in size. The first three dust size bins can be coated by sulfate and nitrate aerosols (Bauer & Koch, 2005). The scheme treats sulfate, nitrate, ammonium, carbonaceous aerosols (black carbon and organic carbon, including the NO_x-dependent formation of secondary organic aerosol (SOA) and methanesulfonic acid formation), dust and sea-salt. The model includes secondary organic aerosol production, as

https://doi.org/10.5194/acp-2020-1296
Preprint. Discussion started: 7 January 2021

described by Tsigaridis and Kanakidou, (2007). OMA only includes the first indirect effect, in which the aerosol number concentration that impacts clouds is obtained from the aerosol mass as described in (Menon & Rotstayn, 2006). In addition to OMA, we have also conducted a non-interactive tracers (NINT: Kelley et al., 2020) simulation from 1850 to 2014, with noninteractive (through monthly varying) fields of radiatively active components (ozone and multiple aerosol species) read in from previously calculated offline fields from the OMA version of the model, ran using the Atmospheric Model Intercomparison Project (AMIP) configuration in Bauer et al. (2020) as described in Kelley et al. (2020). The NINT model includes a tuned aerosol indirect effect following Hansen et al. (2005).

The natural emissions of sea salt, dimethylsulfide (DMS), isoprene and dust are calculated interactively. Anthropogenic dust sources are not represented in GISS-E2.1. Dust emissions vary spatially and temporally only with the evolution of climate variables like wind speed and soil moisture (Miller et al., 2006). The AMIP type simulations (see section 2.3) uses prescribed sea surface temperature (SST) and sea ice fraction during the recent past (Rayner et al., 2003).

2.2. Emissions

In this study, we have used two different emission datasets; the ECLIPSE V6b (Höglund-Isaksson et al.,2020; Klimont et al., 2021), which has been developed with support of the EU-funded Action on Black Carbon in the Arctic (EUA-BCA) and used in the framework of the ongoing AMAP Assessment (AMAP, 2021), referred to as *Eclipse* in this paper, and the CEDS emissions (Hoesly et al., 2018; Feng et al.,2020) combined with selected Shared Socio-economic Pathways (SSP) scenarios used in the CMIP6 future projections (Eyring et al., 2016), collectively referred to as *CMIP6* in this paper.

2.2.1. EclipseV6b emissions

The ECLIPSE V6b emissions dataset is a further evolution of the scenarios established in the EU funded ECLIPSE project (Stohl et al., 2015; Klimont et al., 2017). It has been developed with the global implementation of the GAINS (Greenhouse gas – Air pollution Interactions and Synergies) model (Amann et al., 2011). The GAINS model includes all key air pollutants and Kyoto greenhouse gases, where emissions are estimated for nearly 200 country-regions and several hundred source-sectors representing anthropogenic emissions. For this work, annual emissions were spatially distributed on 0.5°x0.5° lon-lat grids for nine sectors: energy, industry, solvent use, transport, residential combustion, agriculture, open burning of agricultural waste, waste treatment, gas flaring and venting, and international shipping. A monthly pattern for each gridded layer was provided at a 0.5°x0.5° grid level. The ECLIPSE V6b dataset, used in this study, includes an estimate for 1990 to 2015 using statistical data and two scenarios extending to 2050 that rely on the same energy projections from the World Energy Outlook 2018 (IEA, 2018) but have different assumptions about the implementation of air pollution reduction technologies, as described below.

https://doi.org/10.5194/acp-2020-1296
Preprint. Discussion started: 7 January 2021

Atmospheric Chemistry and Physics
Discussions

The Current Legislation (CLE) scenario assumes efficient implementation of the current air pollution legislation committed before 2018, while the Maximum Feasible Reduction (MFR) scenario assumes implementation of best available emission reduction technologies included in the GAINS model. The technology implementation pace in the MFR scenario includes constraints resulting from age structure and typical lifetime of technologies but no constraints resulting from possible economic implications of required large investment in emission reduction technology. The assumptions and the details for the CLE and MFR scenarios (as well as other scenarios developed within the ECLIPSE V6b family) can be found in Höglund-Isaksson et al. (2020) and Klimont et al. (in preparation).

The MFR scenario demonstrates the additional reduction potential of SO_2 emissions by up to 60% and 40%, by 2030 for Arctic Council member and observer countries respectively, with implementation of best available technologies mostly in the energy and industrial sectors and to a smaller extent via measures in the residential sector. The Arctic Council member countries' maximum reduction potential could be fully realized by 2030 whereas in the observer countries additional reductions of 15% to 20% would remain to be achieved between 2030 and 2050.

2.2.2. CMIP6 emissions

The CMIP6 emission datasets include a historical time series generated by the Community Emissions Data System (CEDS) for anthropogenic emissions (Hoesly et al., 2018; Feng et al., 2020), open biomass burning emissions (van Marle et al., 2010), and the future emission scenarios driven by the assumptions embedded in the Shared Socioeconomic Pathways (SSPs) and Representative Concentration Pathways (RCPs) (Riahi et al., 2017) that include specific air pollution storylines (Rao et al., 2017). Gridded CMIP6 emissions are aggregated to nine sectors: agriculture, energy, industrial, transportation, residential–commercial–other, solvents, waste, international shipping, and aircraft. SSP data for future emissions from integrated assessment models (IAMs) are first harmonized to a common 2015 base-year value by the native model per region and sector. This harmonization process adjusts the native model data to match the 2015 starting year values with a smooth transition forward in time, generally converging to native model results (Gidden et al., 2018). The production of the harmonized future emissions data is described in Gidden et al. (2019).

2.2.3. Implementation of the emissions in the GISS-E2.1

In the GISS-E2.1 Eclipse simulations, the non-methane volatile organic carbons (NMVOC) emissions are chemically speciated assuming the SSP2-4.5 VOC composition profiles. The CMIP6 emissions have been pre-processed to include the agricultural waste burning emissions from the EclipseV6b dataset, while the rest of the biomass burning emissions are taken from the CMIP6 emissions. In addition to the biomass burning emissions, the aircraft emissions are also taken from the CMIP6 database to be used in the Eclipse simulations. As seen in Figure 1, the emissions are consistently higher in the CMIP6 compared to the Eclipse emissions. The main differences in the two datasets are mainly over south-east Asia (not shown) . The CMIP6 emissions are also consistently higher on a sectoral basis compared to

https://doi.org/10.5194/acp-2020-1296
Preprint. Discussion started: 7 January 2021

the Eclipse emissions. The figure shows that for air pollutant emissions, the CMIP6 SSP1-2.6 scenario and the Eclipse MFR scenario follow each other closely, while the Eclipse CLE scenario is comparable with the CMIP6 SSP2-4.5 scenario for most pollutants; that is to some extent owing to the fact that the CO_2 trajectory of the Eclipse CLE and the SSP2-4.5 are very similar (not shown). A more detailed discussion of differences between historical Eclipse and CMIP6 as well as CMIP6 scenarios are provided in Klimont et al. (in preparation).

2.3. Simulations

In order to contribute to the AMAP Assessment report (AMAP, 2021), the GISS-E2.1 model participated with AMIP-type simulations, which aim to assess the trends of Arctic air pollution and climate change in the recent past, as well as with fully-coupled climate simulations. Five fully-coupled Earth system models (ESMs) simulated the future (2015-2050) changes of atmospheric composition and climate in the Arctic (>60°N), as well as over the globe. We have carried out two AMIP-type simulations, one with winds nudged to NCEP (standard AMIP-type simulation in AMAP) and one with freely varying winds, where both simulations used prescribed SSTs and sea-ice (Table 1). In the fully-coupled simulations, we carried out two sets of simulations, each with three ensemble members, that used the CLE and MFR emission scenarios. Each simulation in these two sets of scenarios were initialized from a set of three fully-coupled ensemble recent past simulations (1990-2014) to ensure a smooth continuation from CMIP6 to Eclipse emissions.

In addition to the AMAP simulations, we have also conducted CMIP6-type simulations in order to compare the climate aerosol burdens and their impacts on radiative forcing and climate impacts with those from the AMAP simulations. As seen in Table 1, we have conducted one transient fully-coupled simulation from 1850 to 2014, and a number of future scenarios.

2.4. Observations

The GISS-E2.1 ensemble has been evaluated against surface observations of BC, OC and SO_4^{2-}, ground-based and satellite-derived AOD 550 nm, as well as surface and satellite observations of surface air temperature, precipitation, sea surface temperature, sea-ice extent, cloud fraction, and liquid and ice water content in 1995-2014 period. The surface monitoring stations used to evaluate the simulated aerosol levels have been listed in Table S1 and S2 in the supplementary materials.

2.4.1. Aerosols

Measurements of speciated particulate matter (PM), black carbon (BC), sulfate (SO_4^{2-}), and organic carbon (OC) come from three major networks: the Interagency Monitoring of Protected Visual Environments (IMPROVE) for the United States; the European Monitoring and Evaluation Programme (EMEP) for Europe; and the Canadian Air Baseline Measurements (CABM) for Canada (Table S1 and S2). In addition to these monitoring networks, BC, OC, and SO_4^{2-} measurements from individual Arctic stations were used in this study. The individual Arctic stations are Fairbanks and Utqiagvik, Alaska (part of IMPROVE, though their measurements were obtained from their PIs); Gruvebadet and Zeppelin mountain (Ny Alesund), Norway; Villum Research Station, Greenland; and Alert, Nunavut (the latter being an observatory in Global Atmospheric Watch-WMO, and a part of CABM). The measurement techniques are briefly described in the supplement.

AOD at 500 nm from the AErosol RObotic NETwork (AERONET, Holben et al., 1998) was interpolated to 550 nm AOD using the Ångström formula (Ångström, 1929). We also used a new merged AOD product developed by Sogacheva et al. (2020) using AOD from different satellite-based products. According to Sogacheva et al. (2020), this merged product could provide a better representation of temporal and spatial distribution of AOD. However, it is important to note that the monthly aggregates of observations for both AERONET and the satellite products depend on availability of data and are not likely to be the true aggregate of observations for a whole month when only few data points exist during the course of a month. In addition, many polar orbiting satellites take one observation during any given day, and typically at the same local time. Nevertheless, these data sets are key observations currently available for evaluating model performances. Information about the uncertain nature of AOD observations can be found in previous studies (e.g. Sayer et al., 2018; Sayer and Knobelspiesse, 2019; Wei et al., 2019; Schutgens et al., 2020, Schutgens, 2020; Sogacheva et al., 2020).

2.4.2. Surface air temperature, precipitation, and sea-ice

Surface air temperature and precipitation observations used in this study are from University of Delaware gridded monthly mean data sets (UDel; Willmott and Matsuura, 2001). UDel's 0.5° resolution gridded data sets are based on interpolations from station-based measurements obtained from various sources including the Global Historical Climate Network, the archive of Legates and Willmott and others. The Met Office Hadley Center's sea ice and sea surface temperature (HadISST; Rayner et al., 2003) was used for evaluating model simulations of sea ice and SSTs. HadISST data is an improved version of its predecessor known as global sea ice and sea surface temperature (GISST). HadISST data is constructed using information from a variety of data sources such as the Met Office Marine Database, Comprehensive Ocean-Atmosphere Data Set, passive microwave remote sensing retrieval and sea ice charts.

2.4.3. Satellite observations used for cloud fraction and cloud liquid water and ice water

The Advanced Very High Resolution Radiometer (AVHRR-2) sensors onboard the NOAA and EUMETSAT polar orbiting satellites have been flying since the early 1980s. These data have been instrumental in providing the scientific community with climate data records spanning nearly four decades. Tremendous progress has been made in recent decades in improving, training and evaluating the cloud property retrievals from these AVHRR sensors. In this study, we use the retrievals of total cloud fraction from the second edition of EUMETSATs Climate Monitoring Satellite Application Facility (CM SAF) Cloud, Albedo

https://doi.org/10.5194/acp-2020-1296
Preprint. Discussion started: 7 January 2021

Atmospheric Chemistry and Physics Discussions
Open Access
EGU

and surface Radiation data set from AVHRR data (CLARA-A2, Karlsson et al., 2017). This cloud property climate data record is available for the period 1982-2018. Its strengths and weaknesses and inter-comparison with the other similar climate data records are documented in Karlsson and Devasthale (2018). Further data set documentation including Algorithm Theoretical Basis and Validation reports can be found in Karlsson et al. (2017).

Cloud liquid and ice water path estimates derived from the cloud profiling radar on board CloudSat (Stephens et al., 2002) and constrained with another sensor onboard NASA's A-Train constellation, MODIS-Aqua (Platnick et al., 2015), are used for the model evaluation. These Level 2b retrievals, available through 2B-CWC-RVOD product (Version 5), for the period 2007-2016 are analysed. This constrained version is used instead of its radar-only counterpart, as it uses additional information about visible cloud optical depths from MODIS, leading to better estimates of cloud liquid water paths. Because of this constraint the data are available only for the day-lit conditions, and hence, are missing over the polar regions during the respective winter seasons. The theoretical basis for these retrievals can be found in http://www.cloudsat.cira.colostate.edu/sites/default/files/products/files/2B-CWC-RVOD_PDICD.P1_R05.rev0_.pdf (last access: October 26th 2020). Being an active cloud radar, CloudSat provides orbital curtains with a swath width of just about 1.4 km. Therefore, the data are gridded at 5°x5° to avoid too many gaps or patchiness and to provide robust statistics.

3. Results

3.1. Evaluation

The simulations are compared against surface measurements of BC, OC, SO_4^{2-} and AOD, as well as surface and satellite measurements of surface air temperature, precipitation, sea surface temperature, sea-ice extent, total cloud fraction, liquid water path, and ice water path described in section 2.4, by calculating the correlation coefficient (*r*) and normalized mean bias (*NMB*).

3.1.1. Aerosols

The recent past simulations are for BC, OC, SO_4 and AOD (Table 2) against available surface measurements, where individual time series for different stations are accumulated per species in order to get an Arctic evaluation of the model. In addition to Table 2, the climatological mean (1995-2014) of the observed and simulated monthly surface concentrations of BC, OC, SO_4^{2-} and AOD at 550 nm (note that AOD is averaged over 2008, 2009 and 2014) are shown in Figure 2. The AOD observation data for years 2008, 2009, and 2014 are used in order to keep the comparisons in line with the multi-model evaluations being carried out in the AMAP assessment report (AMAP, 2021). We also provide spatial distributions of the NMB, calculated as the mean of all simulations for BC, OC, SO_4 and AOD in Figure 3. The statistics for the individual stations are provided in the Supplementary Material, Tables S3-S6. Results showed overall an underestimation of aerosol species over the Arctic, as discussed below. Surface BC levels are underestimated at all Arctic stations from 15% to

https://doi.org/10.5194/acp-2020-1296
Preprint. Discussion started: 7 January 2021

Atmospheric Chemistry and Physics
Discussions

90%. Surface OC levels are also underestimated from -5% to -70%, except for a slight overestimation over Karvatn (<1%) and a large overestimation of 90% over Trapper Creek. Surface SO_4^{2-} concentrations are also consistently underestimated from -10% to -70%, except for Villum Research Station over northeastern Greenland where there is an overestimation of 45%. Finally AODs are also underestimated over all stations from 20% to 60%. Such underestimations at high latitudes have also been reported by many previous studies (e.g. Skeike et al., 2011; Eckhardt et al., 2015; Lund et al., 2017, 2018; Schacht et al., 2019; Turnock et al., 2020), pointing to a variety of reasons including uncertainties in emission inventories, errors in the wet and dry deposition schemes, the absence or underrepresentation of new aerosol formation processes, and the coarse resolution of global models leading to errors in emissions and simulated meteorology. Turnock et al. (2020) evaluated the air pollutant concentrations in the CMIP6 models, including the GISS-E2.1 ESM, and found that observed surface $PM_{2.5}$ concentrations are consistently underestimated in CMIP6 models by up to 10 μg m^{-3}, particularly for the Northern Hemisphere winter months, with the largest model diversity near natural emission source regions and the Polar regions.

The BC levels are largely underestimated in simulations by 50% (CMIP6_Cpl_Hist) to 67% (Eclipse_AMIP). The CMIP6 simulations have lower bias compared to EclipseV6b simulations due to higher emissions in the CMIP6 emission inventory (Figure 1). Within the EclipseV6b simulations, the lowest bias (-57%) is calculated for the Eclipse_AMIP_NCEP simulation, while the free climate and coupled simulations showed a larger underestimation (>62%), which can be attributed to a better simulation of transport to the Arctic when nudged winds are used. The Eclipse simulations also show that the coupled simulations had slightly smaller biases (*NMB*=-63%) compared to the AMIP-type free climate simulation (AMIP-OnlyAtm: *NMB*=-67%). The climatological monthly variation of the observed levels is poorly reproduced by the model with *r* values around 0.3. BC levels are mainly underestimated in winter and spring, while the summer levels are well captured by the majority of the simulations (Figure 2).

Surface OC concentrations are underestimated from 8% (Eclipse_AMIP_NCEP) to 35% (Eclipse_AMIP) by the Eclipse ensemble, while the CMIP6_Cpl_Hist simulation overestimated surface OC by 13%. The Eclipse simulations suggest that the nudged winds lead to a better representation of transport to the Arctic, while the coupled simulations had smaller biases compared to the AMIP-type free climate simulation (AMIP-OnlyAtm), similar to BC. The climatological monthly variation of the observed concentrations are reasonably simulated, with *r* values between 0.51 and 0.69 (Table 2). The climatological monthly variation of the OC levels are also well simulated in all seasons (Figure 2).

Surface SO_4^{2-} levels are simulated with a smaller bias compared to the BC levels, however still underestimated by 40% (CMIP6_Cpl_Hist) to 53% (Eclipse_AMIP_NCEP). The Eclipse_AMIP_NCEP simulation is biased higher (NMB=-53%) compared to the Eclipse_AMIP (NMB=-50%), probably due to higher cloud fraction simulated by the nudged version (see section 3.1.6). The climatological monthly variation of observed SO_4^{2-} concentrations are reasonably simulated in all simulations (r=0.65-0.74). The observed

https://doi.org/10.5194/acp-2020-1296
Preprint. Discussion started: 7 January 2021

springtime maximum is well captured by the GISS-E2.1 ensemble, with underestimations in all seasons (Figure 2). The clear sky AOD over the Aeronet stations in the Arctic region is underestimated by 33% (Eclipse_AMIP) to 47% (Eclipse_CplHist1). Similar negative biases are found with comparison to the satellite based AOD product (Table 2). The climatological monthly variation is poorly captured with *r* values between -0.07 to 0.07 compared to AERONET AOD and 0 to 0.13 compared to satellite AOD. The simulations could not represent the climatological monthly variation of the observed AERONET AODs (Figure 2).

3.1.2. Climate

The different simulations are evaluated against a set of climate variables and the statistics are presented in Table 3 and in Figures 4 and 5. The climatological mean (1995-2014) monthly Arctic surface air temperatures are slightly overestimated by up to 0.55 °C in the AMIP simulations, while the coupled ocean simulations underestimate the surface air temperatures by up to -0.17 °C. All simulations were able to reproduce the monthly climatological variation with *r* values of 0.99 and higher (Figure 4). The monthly mean precipitation has been underestimated by around 50% by all simulations (Table 3), with largest biases during the summer and autumn (Figure 4). The observed monthly climatological mean variation was very well simulated by all simulations, with *r* values between 0.80 and 0.90.

Arctic SSTs are largely underestimated by the ocean-coupled simulation up to -1.96 °C, while the atmosphere-only runs underestimated SSTs by -1.5 °C (Table 3). The monthly climatological mean variation is well captured with *r* values above 0.99 (Table 3, Figure 4), with a similar cold bias in almost all seasons. The sea-ice extent was overestimated by all coupled simulations by about 12%, while the AMIP-type Eclipse simulations slightly underestimated the extent by 3% (Table 3). The observed variation was also very well captured with very high *r* values. The winter and spring biases were slightly higher compared to the summer and autumn biases (Figure 4).

All simulations overestimated the climatological (1995-2014) mean total cloud fraction by 21% to 25% during the extended winter months (October through February). The largest biases were simulated by the atmosphere-only simulations, with the nudged simulation having the largest bias (*NMB*=25%). The coupled model simulations are closer to the observations during the recent past. On the other hand, the climatology of the cloud fraction was best simulated by the nudged atmosphere-only simulation (Eclipse_AMIP_NCEP) with a *r* value of 0.40, while other simulations showed a poor performance (*r*=-0.17 to +0.10), except for the summer where the bias is lowest (Figure 5). The evaluation against CALIPSO data however shows much smaller biases (*NMB* = +3% to +6%). This decrease in overestimation is due to the strong underestimation of Arctic wintertime cloud formation by AVHRR CLARA-A2 observations due to difficulties in separating cold and bright ice/snow surfaces from clouds (Karlsson et al., 2017), leading to larger positive bias calculated for the model.

Figure 5 shows the evaluation of the simulations with respect to LWP and IWP. It has to be noted here that to obtain a better estimate of the cloud water content, the CloudSat

https://doi.org/10.5194/acp-2020-1296
Preprint. Discussion started: 7 January 2021

observations were constrained with MODIS observations which resulted in a lack of data during the months with darkness (Oct-Mar) over the Arctic (see Section 2.4.3). Hence, we present the results for the polar summer months only. As seen in Figure 5, all simulations overestimated the climatological (2007-2014) mean Polar summer LWP by up to almost 75%. The smallest bias (14%) is calculated for the nudged atmosphere-only (Eclipse_OnlyAtm_NCEP), while the coupled simulations had biases of 70% or more. Observations show a gradual increase in the LWP, peaking in July, whereas the model simulates a more constant amount for the nudged simulation and a slightly decreasing tendency for the other configurations. All model simulations overestimate LWP during the spring months. The atmosphere-only nudged simulations tend to better simulate the observed LWP during the summer months (June through September). The coupled simulations, irrespective of the emission dataset used, are closer to observations only during the months of July and August.

The climatological (2007-2014) mean Polar summer IWP is slightly better simulated compared to the LWP, with biases within -60% with the exception of the nudged Eclipse (Eclipse_AMIP_NCEP) simulation (*NMB*=-74%). All simulations simulated the monthly variation well, with *r* values of 0.95 and more.

In the Arctic, the net cloud forcing at the surface changes sign from positive to negative during the polar summer (Kay and L'Ecuyer, 2013). This change typically occurs in May driven mainly by shortwave cooling at the surface. Since the model simulates the magnitude of the LWP reasonably, particularly in summer, the negative cloud forcing can also be expected to be realistic in the model (e.g. Gryspeerdt et al. 2019). Furthermore, the aerosol and pollution transport into the Arctic typically occurs in the lowermost troposphere where liquid water clouds are prevalent during late spring and summer seasons. The interaction of ice clouds with aerosols is, however, more complex, as ice clouds could have varying optical thicknesses, with mainly thin cirrus in the upper troposphere and relatively thicker clouds in the layers below. Without the knowledge on the vertical distribution of optical thickness, it is difficult to infer the potential impact of the underestimation of IWP on total cloud forcing and their implications.

3.2. Burdens

The recent past and future Arctic column burdens for BC, OC and SO_4^{2-} for the different scenarios and emissions are provided in Figure 6. The BC and SO_4^{2-} burdens started decreasing from the 1990s, while OC burden remains relatively constant, although there is large year-to-year variability in all simulations. All figures show a decrease in burdens after 2015, except for the SSP3-7.0 scenario, where the burdens remain close to the 2015 levels. The high variability in BC and OC burdens over the 2000's are due to the biomass burning emissions from GFED, which have not been harmonised with the no-satellite era. It should also be noted that these burdens can be underestimated considering the negative biases calculated for the surface concentrations and in particular for the AODs reported in Table 2 and Tables S2-6.

https://doi.org/10.5194/acp-2020-1296
Preprint. Discussion started: 7 January 2021

Atmospheric Chemistry and Physics Discussions

All simulations show a significant negative BC burden trend (slope = -0.025±0.003 kTon yr^{-1}) over the Arctic between 1990-2014, except for the CMIP6_Cpl_Hist, which shows a slight non-significant increasing trend of 0.007 kTon yr^{-1}, which can be attributed to the large increase in global anthropogenic BC emissions in CMIP6 after year 2000 (Figure 1). The Eclipse ensemble also shows that the 1990-2010 mean BC burden is simulated to be similar (3.4 kTon) in the coupled and AMIP-type simulations, while the nudged AMIP simulation calculates a slightly higher burden (3.7 kTon). This can be attributed to a better resolved transport of aerosols to the Arctic in the nudged simulation, as suggested by the model evaluation (Table 2). From 2015 onwards, all simulations show a statistically significant negative trend in the Arctic BC burden. The Eclipse simulations show a smaller negative in the trend (-0.03±0.01 kTon yr^{-1}) compared to the CMIP6 simulations (-0.04±0.03 kTon yr^{-1}). The Eclipse CLE simulations calculate a negative trend by -0.02±0.00 kTon yr^{-1}, leading to a 1.1 kTon decrease in the 2030-2050 mean compared to the 1990-2010 mean, while the decrease is larger in the MFR scenario (-0.04±0.00 kTon yr^{-1}), leading to decrease of 2.3 kTon in of 2030-2050 mean. In the CMIP6 simulations, SSP1-2.6 gives the largest reduction by -0.07 kTon yr^{-1} (1.6 kTon decrease in 2030-2050 mean) while the smallest reduction is simulated by the SSP3-7.0 simulation (-0.004 kTon yr^{-1}) with the 2030-2050 mean being 0.5 kTon lower than the 1990-2010 mean. The change in the Eclipse CLE scenario (-1.1 kTon) is comparable with the change of -1 kTon in the SSP2-4.5 scenario, consistent with the projected emission changes in the two scenarios (Figure 1).

The Eclipse simulations show overall a positive trend of OC between 1990 and 2014 (0.03±0.06 kTon yr^{-1}), however this trend is not significant at the 95% confidence level (p=0.5-0.9). The CMIP6_Cpl_Hist simulation gives a larger trend (0.12 kTon yr^{-1}), similar to the BC burden, due to a large increase in global anthropogenic OC emissions in CMIP6 (Figure 1). The nudged AMIP Eclipse simulation calculates the largest 1990-2010 mean OC burden (57 kTon), while the coupled simulation shows a slightly lower 1990-2010 mean burden (55 kTon). This largest OC burden in the Eclipse_AMIP_NCEP simulation is attributed to the largest biogenic SOA calculated in this scenario (Figure S1). The anthropogenic and biogenic contributions to SOA burdens in the coupled Eclipse and CMIP6 recent past simulations imply that the differences in the burdens between the two ensembles can be attributed to the different anthropogenic emissions datasets used in the Eclipse and CMIP6 simulations (Figure S1). The AMIP-type Eclipse run simulates a lower 1990-2010 mean OC burden (50 kTon), attributed to the smallest biogenic SOA burden in this scenario. The Eclipse CLE simulations show a negative trend of -0.20±0.02 kTon yr^{-1} between 2015 and 2050, leading to decrease of 6.2 kTon in 2030-2050 mean burden compared to the 1990-2010 mean, while the MFR simulations show a steeper trend of -0.36±0.02 kTon yr^{-1} (14.9 kTon decrease in 2030-2050 mean vs 1990-2010 mean). The CMIP6 simulations show a much steeper trend of OC by -0.45±0.29 kTon yr^{-1} compared to the Eclipse simulations, with a decrease of 1.9 kTon (SSP3-7.0) to 17 kTon (SSP1-2.6) in the 2030-2050 mean compared to the 1990-2010 mean. Similar to BC burdens, Eclipse CLE and CMIP6 SSP2-4.5 scenarios project similar changes in 2030-2050 mean OC burden (6.9 kTon and 7.8 kTon, respectively).

https://doi.org/10.5194/acp-2020-1296
Preprint. Discussion started: 7 January 2021

Regarding SO_4^{2-} burdens, all simulations show a statistically significant negative trend both in 1990-2014 and in 2015-2050, as seen in Figure 6. Eclipse and CMIP6 simulations show a comparable decrease of Arctic sulfate burdens in the recent past period (-1.16±0.23 T yr^{-1} and -1.09 kTon yr^{-1}, respectively). Both the nudged AMIP-type and coupled simulations showed a 1990-2010 mean SO_4^{2-} burden of 92 kTon, while the AMIP-type simulation showed a larger SO_4^{2-} burden of 95 kTon, attributed to the larger cloud fraction simulated in this model version (Table 2). The Eclipse CLE scenario shows a decrease of -0.14±0.02 kTon/yr in the 2015-2050 period, leading to a decrease of 28 kTon decrease in 2030-2050 mean compared to the 1990-2010 mean, while the MFR shows a very similar trend of -0.15±0.03 kTon yr^{-1}, however with a larger decrease of 2030-2050 mean (-38 kTon). On the other hand, the CMIP6 simulation predicts a much larger decrease of sulfate burdens by -0.49±0.40 kTon yr^{-1} in the future, largely driven by the SSP1-2.6 scenario that gives a decrease of -0.94 kTon yr^{-1}, leading to a decrease of 45 kTon in 2030-2050 mean compared to the 1990-2010 mean.

3.3. Arctic radiative forcing

The TOA aerosol radiative forcings over the Arctic as calculated by the sum of shortwave and longwave TOA forcings from all aerosol species between 1850 and 2050 are presented in Figure 7. The instantaneous forcings are calculated with a double call to the model's radiation code, with and without aerosols. The negative aerosol forcing has increased significantly since 1850 until the 1970's due to an increase in aerosol concentrations. Due to the efforts of mitigating air pollution and thus a decrease in emissions, the forcing became less negative after the 1970's until 2015.

The coupled Eclipse simulations calculated an aerosol TOA radiative forcing of -0.32±0.01 W m^{-2} for the 1990-2010 mean, while AMIP-type Eclipse simulations calculated a forcing of -0.47 W m^{-2} for the same period. For the 2030-2050 period, both the Eclipse CLE and MFR ensembles simulated an aerosol TOA forcing of -0.39±0.01 W m^{-2}. For the anthropogenic aerosols (Figure 7), the Eclipse TOA forcing in 1990-2010 is calculated to be -0.22±0.01 W m^{-2} by the Eclipse ensemble, while in the 2030-2050 period, the TOA anthropogenic forcing (including biomass burning) became more negative in the Eclipse ensemble (-0.24±0.01 W m^{-2}: -0.24±0.00 W m^{-2} and -0.23±0.00 W m^{-2} for CLE and MFR, respectively).

The forcing calculated for the individual aerosol species of BC, OC, SO_4^{2-} and NO_3^- are also investigated separately (Table 4 and Figure 8). The increase in cooling effect of aerosols calculated by the Eclipse ensemble is attributed mainly to the decrease in BC, which is warming the atmosphere as opposed to other aerosol species (Figure 8). More negative forcing is calculated for the OC and NO_3^-, while the SO_4^{2-} forcing is becoming less negative due to large reductions in SO_2 emissions (Figure 1). The net aerosol forcing is therefore slightly more negative. In the CMIP6 ensemble, the BC forcing does not change as much compared to the Eclipse ensemble to counteract the change in impact from SO_4^{2-}, giving a slightly less negative net aerosol forcing. The CMIP6 ensemble also simulates a larger increase in the negative NO_3^- forcing compared to the Eclipse ensemble (Shindell et al.,

https://doi.org/10.5194/acp-2020-1296
Preprint. Discussion started: 7 January 2021

2013). Overall, the changes in the different aerosol species lead to a slightly different but less negative net aerosol forcing by mid-century.

As seen in Table 4, the GISS-E2.1 ensemble calculated a BC TOA direct radiative forcing of up to 0.23 W m^{-2} over the Arctic, with both CMIP6 and Eclipse coupled simulations estimating the highest forcing of 0.23 W m^{-2} for the 1990-2010 mean. This agrees with previous estimates of the BC direct forcing over the Arctic (e.g. Schacht et al., 2019). In the future, the BC forcing is generally decreasing due to lower BC emissions, except for the SSP3-7.0 scenario, where the BC forcing becomes more positive (0.28 W m^{-2}). The 1990-2010 SO_4^{2-} forcing is calculated to be up to -0.39 W m^{-2} in the Eclipse simulations, while the CMIP6 estimates a slightly more negative SO_4^{2-} forcing (-0.4 W m^{-2}). All future simulations show a much less negative SO_4^{2-} forcing in 2030-2050 due to the large reductions in SO_2 emissions. Both OC and NO_3^- forcings are relatively smaller and negative compared to BC and SO_4^{2-} in the 1990-2010 period, and become more negative in 2030-2050.

The NINT and the CMIP6_Cpl_Hist simulations both calculated an aerosol TOA forcing of -0.35 W m^{-2} for the same period, slightly lower than recent estimates (e.g. -0.4 W m^{-2} by Markowicz et al., 2021). For the 2030-2050 period, the CMIP6 future ensemble simulated an aerosol TOA forcing of -0.39±0.02 W m^{-2}, with SSP3-7.0 remaining unchanged compared to the 1990-2010 mean (-0.35 W m^{-2}) and SSP1-2.6 and SSP2-4.5 becoming more negative (-0.40 W m^{-2}). For the anthropogenic aerosols (Figure 7), the CMIP6 TOA forcing in 1990-2010 is calculated to be -0.26 W m^{-2}, while in the 2030-2050 period the TOA anthropogenic aerosol forcing became less negative (-0.25±0.03 W m^{-2}), being ~0.26 W m^{-2} in SSP1-2.6 and SSP2-4.5, and less negative in SSP3-7.0 (-0.21 W m^{-2}). Both ensembles estimated similar TOA aerosol forcing compared to previous studies (e.g. Breider et al., 2017).

The different behaviour in the two ensembles is further investigated by looking at the forcing calculated for the individual aerosol species of BC, OC, SO_4^{2-} and NO_3^- (Table 4 and Figure 8). The increase in cooling effect of aerosols calculated by the Eclipse ensemble is attributed mainly to the decrease in BC as opposed to other aerosol species (Figure 8). More negative forcing is calculated for the OC and NO_3^-, while the SO_4^{2-} forcing is becoming less negative due to large reductions in SO_2 emissions (Figure 1). The net aerosol forcing is therefore slightly more negative. In the CMIP6 ensemble, the BC forcing does not change as much compared to the Eclipse ensemble to counteract the change in impact from SO_4^{2-}, giving a slightly more positive net aerosol forcing. The CMIP6 ensemble also simulates a larger increase in the negative NO_3^- forcing compared to the Eclipse ensemble (Shindell et al., 2013). Overall, the changes in the different aerosol species leads to a higher negative aerosol forcing by mid-century.

Overall, the Eclipse ensemble simulates slightly larger change in the aerosol forcings over the 2015-2050 period, based on the 1990-2010 mean, compared to the CMIP6 ensemble. These changes are consistent with the changes in the aerosol burdens, where Eclipse simulations calculated slightly larger changes in burdens compared to CMIP6 sinnulations. The Eclipse ensemble simulation shows that the aerosol forcing (anthropogenic+natural) anomaly

https://doi.org/10.5194/acp-2020-1296
Preprint. Discussion started: 7 January 2021

becomes negative (-0.09±0.03 W m^{-2}) in 2050 compared to the 2015 anomaly (0.05±0.02 W m^{-2}). The CMIP6 ensemble on the other hand shows that the 2050 anomaly becomes -0.05±0.04 W m^{-2}.

3.4. Climate change

3.4.1. Surface air and sea surface temperatures

The surface air temperature, precipitation, sea surface temperature and sea-ice extent are calculated in the different simulations for the 1990-2050 period. As seen in Figure 9, the Arctic surface air temperatures increase in all scenarios. Between 1990 and 2014, the surface air temperatures over the Arctic increased by 5 °C $decade^{-1}$ (Eclipse_CplHist) to 10 °C $decade^{-1}$ (CMIP6_Cpl_Hist), with a statistically significant ensemble mean trend of 7±2 °C $decade^{-1}$. On the other hand, the observed surface air temperature during 1995-2014 shows a smaller and statistically non-significant increase of 2 °C $decade^{-1}$. From 2015 onwards, surface air temperatures continue to increase significantly by 5±1 °C $decade^{-1}$ in the Eclipse simulations and by 4±1 °C $decade^{-1}$ in the CMIP6 simulations.

The Eclipse ensemble simulated an annual average surface temperature in the Arctic of -7.44±0.94 °C in 1990 while the NINT-Cpl and CMIP6_Cpl_Hist simulated -8.32 °C and -9.21 °C, respectively. The full ensemble simulated an annual average Arctic surface air temperature of -7.87±1.03 °C. The 2030-2050 mean surface air temperatures are projected to increase by 2.1 °C and 2.4 °C compared to the 1990-2010 mean temperature (Figure 9) according to the Eclipse CLE and MFR ensembles, respectively, while the CMIP6 simulation calculated an increase of 1.9 °C (SSP1-2.6) to 2.2 °C (SSP3-7.0). These warmings are smaller compared to the 4.5 - 5 °C warmer 2040 temperatures compared to the 1950-1980 average in the CMIP6 SSP1-2.6, SSP2-4.5 and SSP3-7.0 scenarios, reported by Davy and Outen (2020). It should however be noted that due to the different baselines used in the present study (1990-2010) and the 1950-1980 baseline used in Davy and Outen (2020), it is not possible to directly compare these datasets. Figure 10 shows the spatial distributions of the Arctic surface air temperature change between the 1990-2010 mean and the 2030-2050 mean for the individual Eclipse and CMIP6 future scenarios. All scenarios calculate a warming in the surface air temperatures over the central Arctic, while there are differences over the land areas. The Eclipse CLE and MFR ensembles show similar warming mainly over the Arctic ocean as well as North America and North East Asia and cooling south of Greenland. The latter is a well-known feature of observations and future projections, linked, i.a., to the deep mixed layer in the area and declines in the Atlantic Meridional Circulation (e.g. IPCC, 2014; Menary and Wood, 2018; Keil et al., 2020). There are also differences between the Eclipse and the CMIP6 ensembles as seen in Figure 10. All CMIP6 scenarios show a warming over the central Arctic and a limited cooling over northern Scandinavia, except for the SSP3-7.0 scenario that shows no cooling in the region. The SSP3-7.0-lowNTCF scenario shows an additional cooling over Siberia. These warnings are comparable with earlier studies, such as Samset et al. (2017) estimating a warming of 2.8 °C, attributed to aerosols.

https://doi.org/10.5194/acp-2020-1296
Preprint. Discussion started: 7 January 2021

Following surface air temperatures, sea surface temperatures significantly increase ($p<0.05$) in all simulations (Figure 9). Between 1990-2014, the Eclipse simulations show a warming trend of SSTs by 0.006±0.003 °C yr^{-1}, while the CMIP6 simulations show a much larger increase of 0.012 °C yr^{-1}. Both ensembles underestimated the observed SST trend of 0.017 °C yr^{-1}. The Eclipse CLE and MFR scenarios predict a similar increase of 0.005 °C yr^{-1}, leading to a slight increase of 0.25 °C in 2030-2050 mean surface air temperature compared to the 1990-2010 mean, while the CMIP6 simulations show an increase of 0.003±0.001 °C yr^{-1} , leading to an increase of 0.22 °C to 0.25 °C. Figure S2 shows the spatial distribution of the sea surface temperature change between the 1990-2010 mean and the 2030-2050 mean for the individual Eclipse and CMIP6 future scenarios. All simulations show a cooling of the sea surface over the southern Greenland and north western Atlantic and a warming of the Pacific. The Eclipse scenarios, in particular the MFR scenario, show a warming north of Europe, while this warming is smaller in the CMIP6 simulations, except for the SSP3-7.0-lowNTCF scenario that shows a comparable warming to the Eclipse CLE scenario.

3.4.2. Sea-ice

The Arctic sea-ice extent is found to decrease significantly in all simulations (Figure 9). During the 1990-2014 period, the Eclipse ensemble simulated a decrease of 34 000±5 800 km^2 yr^{-1}, in agreement with the observed decrease of 40 000 km^2 yr^{-1}, while CMIP6_Cpl_Hist simulated a decrease of 70 000 km^2 yr^{-1}, largely overestimating the observations. This overestimation has also been reported for some of the CMIP5 and CMIP6 models (Davy and Outten, 2020). After 2015, the Eclipse CLE ensemble projected a 37 000 ± 12 000 km^2 yr^{-1} decrease while the MFR simulated a slightly higher rate of decrease (-41 000 ± 5 000 km^2 yr^{-1}). The CMIP6 ensemble simulated a slightly smaller decrease rate (-27 000 ± 8 000 km^2 yr^{-1}), with the largest decrease rate simulated by the SSP3-7.0 (-39 000 km^2 yr^{-1}). The evolutions of March and September sea-ice extents are also analysed, representing the Arctic annual maximum and minimum extents, respectively. The Eclipse ensemble projects a decrease of 23 000 ± 11 000 km^2 yr^{-1} in March sea-ice extent during the 2015-2050 period, while the CMIP6 ensemble projects a decrease of 10 000 ± 6000 km^2 yr^{-1} for the same period, both statistically significant. In September, much larger decreases are projected by both ensembles. The Eclipse ensemble simulates a decrease of 64 000 ± 10 000 km^2 yr^{-1} in the 2015-2050 period while the CMIP6 ensemble predicts a decrease of 50 000 ± 20 000 km^2 yr^{-1}.

The 2030-2050 annual mean sea-ice extent is projected to decrease by 1.5 and 1.7 million km^2 compared to the 1990-2010 mean in the Eclipse CLE and MFR scenarios, respectively. The CMIP6 simulations predict a lower decrease of sea-ice extent by 1.2 - 1.5 million km^2. These results are comparable with the results from the CMIP6 models (Davy and Outten, 2020). In the 2030-2050 March mean the sea-ice extent is projected to decrease by 925 000 km^2 in the Eclipse ensemble, while the CMIP6 ensemble projects a decrease of 991 000 km^2. A much larger decrease is projected for the 2030-2050 September mean, being 2.6 million km^2 and 2.3 million km^2 in Eclipse and CMIP6 ensembles, respectively. As seen in Figure 11, the Eclipse ensemble predicts a decrease of September sea-ice fraction by up to 90% in a band marking the maximum retreat of the sea ice line at the end of the summer. The CMIP6

https://doi.org/10.5194/acp-2020-1296
Preprint. Discussion started: 7 January 2021

Atmospheric Chemistry and Physics
Discussions

SSP1-2.6 simulation shows a similar but higher decrease by up to 99%, while the SSP3-7.0 shows an increase of up to 95% over the Canadian Arctic and a decrease of up to 100% over the Siberian Arctic, similar to the Eclipse ensemble. In March (Figure S1), all models agree on a decrease in maximum sea-ice extent at the end of winter over the northern Pacific. In addition, the Eclipse ensemble shows a decrease over the north Atlantic close to Greenland. All simulations show a similar decrease in annual mean sea-ice extent (Figure S2) over the central Arctic, with the CMIP6 ensemble showing also some increase in the sea-ice extent over the Canadian Arctic, that is largest in SSP3-7.0. The retreat in sea-ice extent also led to an increase of oceanic emissions of DMS and sea-salt (Figures S3-S7); however, the increases (Figure S8) are not significant on a 5% significance level. The simulated increase, in particular for the DMS emissions, is slightly larger in the Eclipse ensemble compared to the CMIP6 ensemble, due to a larger decrease of sea-ice extent in the Eclipse ensemble. Also note that GISS-E2.1 is using prescribed and fixed maps of DMS concentration in the ocean. When ocean locations that are year-round under sea-ice at present get exposed, the DMS that would exist in that sea water is not included in the simulations, likely underestimating the increased flux of DMS into the atmosphere as the sea ice retreats.

4. Summary and Conclusions

The GISS-E2.1 earth system model has been used to simulate the recent past (1990-2014) and future (2015-2050) aerosol burdens and their climate impacts over the Arctic. An ensemble of seventeen simulations has been conducted, using historical and future anthropogenic emissions and projections from CMIP6 and ECLIPSE V6b, the latter supporting the ongoing Arctic Monitoring and Assessment Programme.

The evaluation of the recent past simulations shows underestimates of Arctic surface aerosol levels by up to 50%, with the smallest biases calculated for the nudged AMIP-type Eclipse simulations. An exception is SO_4^{2-}, where Eclipse_AMIP_NCEP had the highest bias, due to the high cloud bias that leads to more in-cloud sulfate production from SO_2. The model skill analyses indicate slightly better performance of the CMIP6 version of the GISS-E2.1 model in simulating both the aerosol levels and climate parameters compared to the Eclipse version. In addition, fully-coupled simulations had slightly smaller biases in aerosol levels compared to atmosphere-only simulations (winds not nudged). Results from the various Eclipse ensemble simulations showed that lowest biases in surface aerosols concentrations are calculated for atmosphere only (prescribed sea-ice and sea-surface temperature) simulations with nudged winds.

From 2015 onwards, all simulations show a statistically significant decrease in the Arctic BC, OC and SO_4^{2-} burdens, with the CMIP6 ensemble showing larger reductions in Arctic aerosol burdens compared to the Eclipse ensemble. The Eclipse CLE and the CMIP6 SSP1-2.6 show the largest reductions. Results indicated that the differences in burdens between the two ensembles can be attributed to the different anthropogenic emissions datasets used. Results from the various Eclipse simulations showed that the biogenic SOA contribution to the OC

https://doi.org/10.5194/acp-2020-1296
Preprint. Discussion started: 7 January 2021

burdens was higher in the nudged atmosphere only simulation, compared to the non-nudged and coupled simulations.

The present-day (1990-2010 mean) CMIP6 and Eclipse simulations calculated an aerosol TOA forcing of -0.35 W m^{-2} and -0.32±0.01 W m^{-2}, respectively. For the same period, the atmosphere only (AMIP) Eclipse simulations calculated a much larger aerosol TOA forcing of -0.47 W m^{-2}. For the 2030-2050 period, both the Eclipse ensemble simulated an aerosol TOA forcing of -0.39±0.01 W m^{-2}, of which -0.24±0.01 W m^{-2} are attributed to the anthropogenic aerosols (BC, OC, SO_4^{2-} and NO_3^-). For the same period, the CMIP6 SSP3-7.0 simulated a similar TOA aerosol forcing (-0.35 W m^{-2}) compared to the 1990-2010 mean , while SSP1-2.6 and SSP2-4.5 scenarios simulated a more negative TOA forcing (-0.40 W m^{-2}), of which the anthropogenic aerosols were responsible for -0.26 W m^{-2}). Overall, the Eclipse ensemble simulated slightly larger changes in the aerosol forcings over the 2015-2050 period, relative to the 1990-2010 mean, compared to the CMIP6 ensemble. The differences between the two ensembles are further attributed to differences in the BC and SO_4^{2-} forcings. These results suggest that the different anthropogenic emission projections between the two ensembles and within them lead to only small differences in how the aerosol radiative forcing will evolve in the future over the Arctic.

The scenarios with the largest aerosol reductions, i.e. MFR in the Eclipse and SSP1-2.6 in the CMIP6 ensemble projects a largest warming and sea-ice retreat. Overall, both Eclipse and CMIP6 ensembles show a similar increasing trend of surface air temperatures over the Arctic between 1990 and 2050, with the CMIP ensemble showing a slightly higher warming trend (6±3 °C $decade^{-1}$) compared to the trend calculated by the Eclipse ensemble (5±1 °C $decade^{-1}$). On the other hand, the Eclipse ensemble shows a slightly larger warming of 2030-2050 mean surface air temperatures of 2.1 to 2.5 °C over the Arctic compared to that from the CMIP6 ensemble (1.9 °C to 2-2 °C). The Eclipse ensemble simulates a slightly larger reduction in sea-ice extent in the Eclipse ensemble (-1.5 to -1.7 million km^{-2} in CLE and MFR, respectively) in 2030-2050 mean compared to the reduction in the CMIP6 scenario (-1.3 to -1.6 million km^{-2} in SSP1.2-6 and SSP3-7.0, respectively). However, the changes simulated by the two ensembles are within one standard deviation of each other.

The overall results showed that the aerosol burdens will substantially decrease in the short- to mid-term future, implying improvements in impacts on human health and ecosystems., Results also show that even the scenarios with largest emission reductions, i.e. Eclipse MFR and CMIP6 SSP1-2.6, lead to similar impact on the future Arctic surface air temperatures compared to scenarios with smaller emission reductions. On the other hand, scenarios with very little mitigation such as the CMIP6 SSP3-7.0 leads to much larger sea-ice loss, implying that even though impacts are small in temperatures, high mitigation of aerosols are still necessary to limit sea-ice loss, exacerbating the dominant role played by well-mixed greenhouse gases and underlining the importance of continued greenhouse gas reductions.

Author contributions. UI coordinated the study, conducted the model simulations, as well as model evaluation and analyses of the simulations, and wrote the manuscript. KT and GF supported the model simulations and processing of the Eclipse V6b emissions for the GISS-

https://doi.org/10.5194/acp-2020-1296
Preprint. Discussion started: 7 January 2021

Atmospheric Chemistry and Physics Discussions

E2.1 model. JPF contributed to the plotting of the spatial distributions by further developing the autoimage R package (French, 2017). RM prepared and provided the AOD measurements, as well as the surface air temperature, sea surface temperature and sea-ice data. TM prepared the cloud observation data. CHW prepared the Arctic surface aerosol measurement data. KvS coordinated the experimental setup for the Eclipse simulations in the framework of the ongoing AMAP assessment. ZG prepared and provided the Eclipse V6b anthropogenic emissions. HS and DCT prepared the Villum Research Station aerosol data. JB and PL contributed to analyses of aerosols and climate parameters, respectively, and manuscript writing. All authors contributed to the analyses and interpretation of the results, as well as contributing to the writing of the manuscript.

Competing Interests. The authors declare that they have no conflict of interest.

Special issue statement. This article is part of the special issue "Arctic climate, air quality, and health impacts from short-lived climate forcers (SLCFs): contributions from the AMAP Expert Group".

Acknowledgements. This paper was developed as part of the Arctic Monitoring Assessment Programme (AMAP), AMAP 2021Assessment: Arctic climate, air quality, and health impacts from short-lived climate forcers (SLCFs). HadISST data were obtained from https://www.metoffice.gov.uk/hadobs/hadisst/ and are © British Crown Copyright, Met Office, provided under a Non-Commercial Government Licence http://www.nationalarchives.gov.uk/doc/non-commercial-government-licence/version/2/. UDel_AirT_Precip data provided by the NOAA/OAR/ESRL PSL, Boulder, Colorado, USA, from their Web site at https://psl.noaa.gov/. Alert sulfate data are from Sangeeta and EC & OC data from Lin Huang, respectively, as part of Canadian Aerosol Baseline Measurement (CABM) program at ECCC and would like to thank operators & technicians for collection of filters, calibration and analysis and Canadian Forces Services Alert for the operation of the military base. These datasets are also available on Global Atmospheric Watch program, World Data Center for aerosols, EBAS database (http://ebas.nilu.no/default.aspx).Aside from Alert, Canada's surface air quality data are from the National Atmospheric Pollutant Surveillance network (NAPS: https://open.canada.ca/data/en/dataset/1b36a356-defd-4813-acea-47bc3abd859b).
Fairbanks aerosol measurements are from William Simpson and KC Nattinger. Aside from Fairbanks, Alaskan measurements are from the IMPROVE network. IMPROVE is a collaborative association of state, tribal, and federal agencies, and international partners. The US Environmental Protection Agency is the primary funding source, with contracting and research support from the National Park Service. The Air Quality Group at the University of California, Davis is the central analytical laboratory, with ion analysis provided by Research Triangle Institute, and carbon analysis provided by Desert Research Institute.
European measurements are from the EMEP network, and obtained from the EBAS database (http://ebas.nilu.no). Other European data include the Gruvebadet measurements, for which we acknowledge Mauro Mazzola (mauro.mazzola@cnr.it), Stefania Gilardoni (stefania.gilardoni@cnr.it), and Angelo Lupi (angelo.lupi@cnr.it) from the Institute of Polar Sciences fo Gruvabadet eBC measurements; and Rita Traversi (rita.traversi@unifi.it), Mirko

Severi (mirko.severi@unifi.it), and Silvia Becagli (silvia.becagli@unifi.it) from University of Florence http://www.isac.cnr.it/~radiclim/CCTower/ ?Data:Aerosol; the Zeppelin datasets, for which we acknowledge Vito Vitale and Angelo Lupi (also available on http://ebas.nilu.no); and the Villum Station datasets (www.villumresearchstation.dk) from Henrik Skov (hsk@envs.au.dk; also available in http://ebas.nilo.no). The AERONET AOD measurements were obtained from NASA's Goddard Space Flight Center (https://aeronet.gsfc.nasa.gov/new_web/index.html). The authors acknowledge Dr. L. Sogacheva and AEROSAT team for satellite based merged AOD data.

Financial support. This research has been supported by the Aarhus University Interdisciplinary Centre for Climate Change (iClimate) OH fund (no. 2020-0162731), the FREYA project, funded by the Nordic Council of Ministers (grant agreement no. MST-227-00036 and MFVM-2019-13476), and the EVAM-SLCF funded by the Danish Environmental Agency (grant agreement no. MST-112-00298). KT and GF thank the NASA Modeling, Analysis and Prediction program (MAP) for support. ZK was financially supported by the EU-funded Action on Black Carbon in the Arctic (EUA-BCA) under the EU Partnership Instrument. JPF was partially supported by NSF award 1915277.

References

Abbatt, J. P. D., Leaitch, W. R., Aliabadi, A. A., Bertram, A. K., Blanchet, J.-P., Boivin-Rioux, A., Bozem, H., Burkart, J., Chang, R. Y. W., Charette, J., Chaubey, J. P., Christensen, R. J., Cirisan, A., Collins, D. B., Croft, B., Dionne, J., Evans, G. J., Fletcher, C. G., Galí, M., Ghahremaninezhad, R., Girard, E., Gong, W., Gosselin, M., Gourdal, M., Hanna, S. J., Hayashida, H., Herber, A. B., Hesaraki, S., Hoor, P., Huang, L., Hussherr, R., Irish, V. E., Keita, S. A., Kodros, J. K., Köllner, F., Kolonjari, F., Kunkel, D., Ladino, L. A., Law, K., Levasseur, M., Libois, Q., Liggio, J., Lizotte, M., Macdonald, K. M., Mahmood, R., Martin, R. V., Mason, R. H., Miller, L. A., Moravek, A., Mortenson, E., Mungall, E. L., Murphy, J. G., Namazi, M., Norman, A.-L., O'Neill, N. T., Pierce, J. R., Russell, L. M., Schneider, J., Schulz, H., Sharma, S., Si, M., Staebler, R. M., Steiner, N. S., Thomas, J. L., von Salzen, K., Wentzell, J. J. B., Willis, M. D., Wentworth, G. R., Xu, J.-W., and Yakobi-Hancock, J. D.: Overview paper: New insights into aerosol and climate in the Arctic, Atmos. Chem. Phys., 19, 2527–2560, https://doi.org/10.5194/acp-19-2527-2019, 2019.

AMAP 2021 Assessment: Arctic climate, air quality, and health impacts from short-lived climate forcers (SLCFs).

AMAP, 2015. AMAP Assessment 2015: Black carbon and ozone as Arctic climate forcers. Arctic Monitoring and Assessment Programme (AMAP), Oslo, Norway. vii + 116 pp.

Amann, M., Bertok, I., Borken-Kleefeld, J., Cofala, J., Heyes, C., Höglund-Isaksson, L., Klimont, Z., Nguyen, B., Posch, M., Rafaj, P., Sandler, R., Schöpp, W., Wagner, F., Winiwarter, W.: Cost-effective control of air quality and greenhouse gases in Europe: Modeling and policy applications. Environmental Modelling & Software, 26, (12), 1489-1501, 2011.

https://doi.org/10.5194/acp-2020-1296
Preprint. Discussion started: 7 January 2021

Ångström, A.: On the Atmospheric Transmission of Sun Radiation and on Dust in the Air. Geografiska Annaler, 11, 156-166. doi:10.2307/519399, 1929.

Bauer, S. E., Tsigaridis, K., Faluvegi, G.,Kelley, M., Lo, K. K., & Miller, R. L.,et al.: Historical (1850–2014) aerosol evolution and role on climate forcing using the GISS ModelE2.1contribution to CMIP6. Journal ofAdvances in Modeling Earth Systems,12, e2019MS001978, https://doi.org/10.1029/2019MS001978, 2020.

Bauer, S.E., and Koch, D.: Impact of heterogeneous sulfate formation at mineral dust surfaces on aerosol loads and radiative forcing in the Goddard Institute for Space Studies general circulation model. J. Geophys. Res., 110, D17202, doi:10.1029/2005JD005870, 2005.

Bond, T.C., Doherty, S.J., Fahey, D.W., Forster, P.M. , Berntsen, T., De Angelo, B.J., Flanner, M.G., Ghan, S., Karcher, B., Koch, D., Kinne, S., Kondo, Y., Quiinn, P.K., Sarofim, M.C., Schultz, M.G., Schulz, M., Venkataraman, C., Zhang, H., Zhang, S., Bellouin, N., Guttikunda, S.K., Hopke, P.K., Jacobson, M.Z., Kaiser, J.W., Klimont, Z., Lohmann, U., Schwarz, J.P., Shindell, D., Storelvmo, T., Warren, S.G., Zender, C.S.: Bounding the role of black carbon in the climate system: a scientific assessment, J. Geophys. Res. Atmos., 118 (11), 5380-5552, 10.1002/jgrd.50171, 2013.

Bond, T. C., D. G. Streets, K. F. Yarber, S. M. Nelson, J. H. Woo, and Z. Klimont: A technology-based global inventory of black and organic carbon emissions from combustion, J. Geophys. Res., 109, D14203, doi:10.1029/2003JD003697, 2014.

Boy, M., Thomson, E. S., Acosta Navarro, J.-C., Arnalds, O., Batchvarova, E., Bäck, J., Berninger, F., Bilde, M., Brasseur, Z., Dagsson-Waldhauserova, P., Castarède, D., Dalirian, M., de Leeuw, G., Dragosics, M., Duplissy, E.-M., Duplissy, J., Ekman, A. M. L., Fang, K., Gallet, J.-C., Glasius, M., Gryning, S.-E., Grythe, H., Hansson, H.-C., Hansson, M., Isaksson, E., Iversen, T., Jonsdottir, I., Kasurinen, V., Kirkevåg, A., Korhola, A., Krejci, R., Kristjansson, J. E., Lappalainen, H. K., Lauri, A., Leppäranta, M., Lihavainen, H., Makkonen, R., Massling, A., Meinander, O., Nilsson, E. D., Olafsson, H., Pettersson, J. B. C., Prisle, N. L., Riipinen, I., Roldin, P., Ruppel, M., Salter, M., Sand, M., Seland, Ø., Seppä, H., Skov, H., Soares, J., Stohl, A., Ström, J., Svensson, J., Swietlicki, E., Tabakova, K., Thorsteinsson, T., Virkkula, A., Weyhenmeyer, G. A., Wu, Y., Zieger, P., and Kulmala, M.: Interactions between the atmosphere, cryosphere, and ecosystems at northern high latitudes, Atmos. Chem. Phys., 19, 2015–2061, https://doi.org/10.5194/acp-19-2015-2019, 2019.

Breider, T. J., Mickley, L. J., Jacob, D. J., Ge, C., Wang, J., Payer Sulprizio, M., Croft, B., Ridley, D. A., McConnell, J. R., Sharma, S., Husain, L., Dutkiewicz, V. A., Eleftheriadis, K., Skov, H. and Hopke, P. K.: Multidecadal trends in aerosol radiative forcing over the Arctic: Contribution of changes in anthropogenic aerosol to Arctic warming since 1980, J. Geophys. Res. Atmos., 122(6), 3573–3594, doi:10.1002/2016JD025321, 2017.

Burnett, R., Chena, H., Szyszkowicza, M., Fann, N., Hubbell, B., Pope III, C. A., Apte, J. S., Brauer, M., Cohen, A., Weichenthal, S., Coggins, J., Di Q., Brunekreef B., Frostad, J., Lim, S. S., Kan, H., Walker, K. D., Thurston, G. D., Hayes, R. B., Lim, C. C., Turner, M. C., Jerrett, M., Krewski, D., Gapstur, S. M., Diver, W. R., Ostro, B., Goldberg, D., Crouse, D. L., Martin, R. V., Peters, P., Pinault, L., Tjepkema, M., van Donkelaar, M., Villeneuve, P. J.,

https://doi.org/10.5194/acp-2020-1296
Preprint. Discussion started: 7 January 2021

Miller, A. B., Yin, P., Zhou, M., Wang, L., Janssen, N. A. H., Marra, M., Atkinson, R. W., Tsang, H., Thach, T. Q., Cannon, J. B., Allen, R. T., Hart, J. E., Laden, F., Cesaroni, G., Forastiere, F., Weinmayr, G., Jaensch, A., Nagel, G., Concin, H. and Spadar, J. V., Global estimates of mortality associated with long term exposure to outdoor fine particulate matter. Proceedings of the National Academy of Sciences, 38 (115), pp. 9592–9597. doi: 10.1073/pnas.1803222115. 2018.

Clarke, A.D., and Noone, K.J.: Soot in the Arctic snowpack: A cause for perturbations in radiative transfer, Atmos. Environ., 19, 2045– 2053, 1985.

Davy, R., and Outten, S.: The Arctic Surface Climate in CMIP6: Status and Developments since CMIP5, *J. Climate*, 33 (18), 8047–8068, https://doi.org/10.1175/JCLI-D-19-0990.1, 2020.

Dumont, M., Brun, E., Picard, G. et al.: Contribution of light-absorbing impurities in snow to Greenland's darkening since 2009. Nature Geosci 7, 509–512, https://doi.org/10.1038/ngeo2180, 2014.

Eck, T.F., B.N.Holben, J.S.Reid, O.Dubovik, A.Smirnov, N.T.O'Neill, I.Slutsker, and S.Kinne: Wavelength dependence of the optical depth of biomass burning, urban and desert dust aerosols, J. Geophys. Res., 104, 31 333-31 350, 1999.

Eckhardt, S., Quennehen, B., Olivié, D. J. L., Berntsen, T. K., Cherian, R., Christensen, J. H., Collins, W., Crepinsek, S., Daskalakis, N., Flanner, M., Herber, A., Heyes, C., Hodnebrog, Ø., Huang, L., Kanakidou, M., Klimont, Z., Langner, J., Law, K. S., Lund, M. T., Mahmood, R., Massling, A., Myriokefalitakis, S., Nielsen, I. E., Nøjgaard, J. K., Quaas, J., Quinn, P. K., Raut, J.-C., Rumbold, S. T., Schulz, M., Sharma, S., Skeie, R. B., Skov, H., Uttal, T., von Salzen, K., and Stohl, A.: Current model capabilities for simulating black carbon and sulfate concentrations in the Arctic atmosphere: a multi-model evaluation using a comprehensive measurement data set, Atmos. Chem. Phys., 15, 9413–9433, https://doi.org/10.5194/acp-15-9413-2015, 2015.

Eyring, V., Bony, S., Meehl, G. A., Senior, C. A., Stevens, B., Stouffer, R. J., and Taylor, K. E.: Overview of the Coupled Model Intercomparison Project Phase 6 (CMIP6) experimental design and organization, Geosci. Model Dev., 9, 1937–1958, https://doi.org/10.5194/gmd-9-1937-2016, 2016.

Feng, L., Smith, S. J., Braun, C., Crippa, M., Gidden, M. J., Hoesly, R., Klimont, Z., van Marle, M., van den Berg, M., and van der Werf, G. R.: The generation of gridded emissions data for CMIP6, Geosci. Model Dev., 13, 461–482, https://doi.org/10.5194/gmd-13-461-2020, 2020.

Flanner, M.G., Zender, C.S., Randerson, J.T., and Rasch, P.J.: Present-day climate forcing and response from blackcarbon in snow, J. Geophys. Res., 112, D11202, doi:10.1029/2006JD008003, 2007.

French, J.P.: autoimage: Multiple Heat Maps for Projected Coordinates, The R Journal, 9 (1), 284-297, 2017.

https://doi.org/10.5194/acp-2020-1296
Preprint. Discussion started: 7 January 2021

Gagné, M.-È., Gillett, N.P., and Fyfe, J. C.: Impact of aerosolemission controls on futureArctic sea ice cover, Geo-phys. Res. Lett., 42, 8481–8488,doi:10.1002/2015GL065504, 2015.

Gery, M., Whitten, G.Z., Killus, J.P., and Dodge, M.C.: A photochemical kinetics mechanism for urban and regional scale computer modelling, J.Geophys.Res., 94, 18925-18956, 1989.

Gidden, M. J., Riahi, K., Smith, S. J., Fujimori, S., Luderer, G., Kriegler, E., van Vuuren, D. P., van den Berg, M., Feng, L., Klein, D., Calvin, K., Doelman, J. C., Frank, S., Fricko, O., Harmsen, M., Hasegawa, T., Havlik, P., Hilaire, J., Hoesly, R., Horing, J., Popp, A., Stehfest, E., and Takahashi, K.: Global emissions pathways under different socioeconomic scenarios for use in CMIP6: a dataset of harmonized emissions trajectories through the end of the century, Geosci. Model Dev., 12, 1443–1475, https://doi.org/10.5194/gmd-12-1443-2019, 2019.

Gidden, M. J., Fujimori, S., van den Berg, M., Klein, D., Smith, S. J., van Vuuren, D. P., and Riahi, K.: A methodology and implementation of automated emissions harmonization for use in Integrated Assessment Models, Environ. Modell. Softw., 105, 187–200, 2018.

Graversen R, Langen P.L.: On the Role of the Atmospheric Energy Transport in 2xCO2-Induced Polar Amplification in CESM1. Journal of Climate, 32(13), 3941-3956, 2019.

Gryspeerdt, E., Goren, T., Sourdeval, O., Quaas, J., Mülmenstädt, J., Dipu, S., Unglaub, C., Gettelman, A., and Christensen, M.: Constraining the aerosol influence on cloud liquid water path, Atmos. Chem. Phys., 19, 5331–5347, https://doi.org/10.5194/acp-19-5331-2019, 2019.

Hansen, J., M. Sato, R. Ruedy, L. Nazarenko, A. Lacis, G.A. Schmidt, G. Russell, I. Aleinov, M. Bauer, S. Bauer, N. Bell, B. Cairns, V. Canuto, M. Chandler, Y. Cheng, A. Del Genio, G. Faluvegi, E. Fleming, A. Friend, T. Hall, C. Jackman, M. Kelley, N.Y. Kiang, D. Koch, J. Lean, J. Lerner, K. Lo, S. Menon, R.L. Miller, P. Minnis, T. Novakov, V. Oinas, J.P. Perlwitz, J. Perlwitz, D. Rind, A. Romanou, D. Shindell, P. Stone, S. Sun, N. Tausnev, D. Thresher, B. Wielicki, T. Wong, M. Yao, and S. Zhang: Efficacy of climate forcings. J. Geophys. Res., 110, D18104, doi:10.1029/2005JD005776, 2005.

Hoesly, R. M., Smith, S. J., Feng, L., Klimont, Z., Janssens-Maenhout, G., Pitkanen, T., Seibert, J. J., Vu, L., Andres, R. J., Bolt, R. M., Bond, T. C., Dawidowski, L., Kholod, N., Kurokawa, J.-I., Li, M., Liu, L., Lu, Z., Moura, M. C. P., O'Rourke, P. R., and Zhang, Q.: Historical (1750–2014) anthropogenic emissions of reactive gases and aerosols from the Community Emissions Data System (CEDS), Geosci. Model Dev., 11, 369–408, https://doi.org/10.5194/gmd-11-369-2018, 2018.

Holben B.N., T.F.Eck, I.Slutsker, D.Tanre, J.P.Buis, A.Setzer, E.Vermote, J.A.Reagan, Y.Kaufman, T.Nakajima, F.Lavenu, I.Jankowiak, and A.Smirnov: AERONET - A federated instrument network and data archive for aerosol characterization, Rem. Sens. Environ., 66, 1-16, 1998.

Höglund-Isaksson, L., Gómez-Sanabria, A., Klimont, Z., Rafaj, P., Schöpp, W.: Technical potentials and costs for reducing global anthropogenic methane emissions in the 2050

https://doi.org/10.5194/acp-2020-1296
Preprint. Discussion started: 7 January 2021

Atmospheric Chemistry and Physics
Discussions

timeframe –results from the GAINS model. Environmental Research Communications, 2 (2), 2020.

International Energy Agency (IEA): World Energy Outlook 2018, 661 pp., ISBN 978-92-64-30677-6, 2018.

IPCC, 2014: Climate Change 2014: Synthesis Report. Contribution of Working Groups I, II and III to the Fifth Assessment Report of the Intergovernmental Panel on Climate Change [Core Writing Team, R.K. Pachauri and L.A. Meyer (eds.)]. IPCC, Geneva, Switzerland, 151 pp.

IPCC, 2013: Climate Change 2013: The Physical Science Basis. Contribution of Working Group I to the Fifth Assessment Report of the Intergovernmental Panel on Climate Change [Stocker, T.F., D. Qin, G.-K. Plattner, M. Tignor, S.K. Allen, J. Boschung, A. Nauels, Y. Xia, V. Bex and P.M. Midgley (eds.)]. Cambridge University Press, Cambridge, United Kingdom and New York, NY, USA, 1535 pp.

Jacobson, M. Z.: Strong radiative heating due to the mixing state of black carbon in the atmospheric aerosols, Nature, 409, 695–698, 2001.

Karlsson, K.-G., Devasthale, A: Inter-Comparison and Evaluation of the Four Longest Satellite-Derived Cloud Climate Data Records: CLARA-A2, ESA Cloud CCI V3, ISCCP-HGM, and PATMOS-x. Remote Sens. 2018, 10, 1567.

Karlsson, K.-G., Anttila, K., Trentmann, J., Stengel, M., Fokke Meirink, J., Devasthale, A., Hanschmann, T., Kothe, S., Jääskeläinen, E., Sedlar, J., Benas, N., van Zadelhoff, G.-J., Schlundt, C., Stein, D., Finkensieper, S., Håkansson, N., and Hollmann, R.: CLARA-A2: the second edition of the CM SAF cloud and radiation data record from 34 years of global AVHRR data, Atmos. Chem. Phys., 17, 5809–5828, https://doi.org/10.5194/acp-17-5809-2017, 2017.

Karlsson, Karl-Göran; Anttila, Kati; Trentmann, Jörg; Stengel, Martin; Meirink, Jan Fokke; Devasthale, Abhay; Hanschmann, Timo; Kothe, Steffen; Jääskeläinen, Emmihenna; Sedlar, Joseph; Benas, Nikos; van Zadelhoff, Gerd-Jan; Schlundt, Cornelia; Stein, Diana; Finkensieper, Stephan; Håkansson, Nina; Hollmann, Rainer; Fuchs, Petra; Werscheck, Martin (2017): CLARA-A2: CM SAF cLoud, Albedo and surface RAdiation dataset from AVHRR data - Edition 2, Satellite Application Facility on Climate Monitoring, https://doi.org/10.5676/EUM_SAF_CM/CLARA_AVHRR/V002 (last access: October 26th 2020).

Kay, J., and L'Ecuyer, T.: Observational constraints on Arctic Ocean clouds and radiative fluxes during the early 21st century. Journal of Geophysical Research: Atmospheres. 118. 10.1002/jgrd.50489, 2013.

Keil, P., Mauritsen, T., Jungclaus, J. *et al.* Multiple drivers of the North Atlantic warming hole. *Nat. Clim. Chang.* 10, 667–671, https://doi.org/10.1038/s41558-020-0819-8, 2020.

Kelley, M., Schmidt, G. A., Nazarenko, L. S., Bauer, S. E., Ruedy, R., Russell, G. L., et al.: GISS-E2.1: Configurations and climatology. Journal of Advances in Modeling Earth Systems, 12, e2019MS002025. https://doi.org/10.1029/2019MS002025, 2020.

Klimont, Heyes, Rafaj, Schoepp, Purohit, Cofala, Hoglund-Isaksson, Wagner,...et al. Global scenarios of anthropogenic emissions of air pollutants: ECLIPSE (in preparation for GMD)

Klimont, Z., Kupiainen, K., Heyes, C., Purohit, P., Cofala, J., Rafaj, P., Borken-Kleefeld, J., and Schöpp, W.: Global anthropogenic emissions of particulate matter including black carbon, Atmos. Chem. Phys., 17, 8681–8723, https://doi.org/10.5194/acp-17-8681-2017, 2017.

Lamarque, J.-F., Bond, T. C., Eyring, V., Granier, C., Heil, A., Klimont, Z., Lee, D., Liousse, C., Mieville, A., Owen, B., Schultz, M. G., Shindell, D., Smith, S. J., Stehfest, E., Van Aardenne, J., Cooper, O. R., Kainuma, M., Mahowald, N., McConnell, J. R., Naik, V., Riahi, K., and van Vuuren, D. P.: Historical (1850–2000) gridded anthropogenic and biomass burning emissions of reactive gases and aerosols: methodology and application, Atmos. Chem. Phys., 10, 7017–7039, https://doi.org/10.5194/acp-10-7017-2010, 2010.

Lelieveld, J., Klingmüller, K., Pozzer, A., Pöschl, U., Fnais, M., Daiber, A., Münzel, T. Cardiovascular disease burden from ambient air pollution in Europe reassessed using novel hazard ratio functions. European Heart Journal 40, 1590-1596. https://doi.org/10.1093/eurheartj/ehz135, 2019.

Lenssen, N. J. L., Schmidt, G. A., Hansen, J. E., Menne, M. J., Persin, A., Ruedy, R. and Zyss, D.: Improvements in the GISTEMP Uncertainty Model. Journal of Geophysical Research: Atmospheres 124: 6307-6326 10.1029/2018jd029522, 2019.

Lewinschal, A., Ekman, A. M. L., Hansson, H. C., Sand, M., Berntsen, T. K., & Langner, J. (2019). Local and remote temperature response of regional SO2 emissions. Atmospheric Chemistry and Physics, 19, 2385– 2403. https://doi.org/10.5194/acp-19-2385-2019

Lund, M. T., Myhre, G., Haslerud, A. S., Skeie, R. B., Griesfeller, J., Platt, S. M., Kumar, R., Myhre, C. L., and Schulz, M.: Concentrations and radiative forcing of anthropogenic aerosols from 1750 to 2014 simulated with the Oslo CTM3 and CEDS emission inventory, Geosci. Model Dev., 11, 4909–4931, https://doi.org/10.5194/gmd-11-4909-2018, 2018.

Lund, M. T., Berntsen, T. K., and Samset, B. H.: Sensitivity of black carbon concentrations and climate impact to aging and scavenging in OsloCTM2-M7, Atmos. Chem. Phys., 17, 6003–6022, https://doi.org/10.5194/acp-17-6003-2017, 2017.

Mahmood, R., von Salzen, K., Norman, A.-L., Galí, M., and Levasseur, M.: Sensitivity of Arctic sulfate aerosol and clouds to changes in future surface seawater dimethylsulfide concentrations, Atmos. Chem. Phys., 19, 6419–6435, https://doi.org/10.5194/acp-19-6419-2019, 2019.

Markowicz, K.M.,Lisok, J., Xian, P.: Simulation of long-term direct aerosol radiative forcing over the arctic within the framework of the iAREA project. Atmospheric Environment, 244, 117882, 2021.

Menary, M.B., Wood, R.A.: An anatomy of the projected North Atlantic warming hole in CMIP5 models. *Clim Dyn* 50, 3063–3080, https://doi.org/10.1007/s00382-017-3793-8, 2018.

https://doi.org/10.5194/acp-2020-1296
Preprint. Discussion started: 7 January 2021

Menon, S., and Rotstayn, L.: The radiative influence of aerosol effects on liquid-phase cumulus and stratus clouds based on sensitivity studies with two climate models, Clim. Dyn., 27, 345– 356, 2006.

Miller, R.L., G.A. Schmidt, L. Nazarenko, S.E. Bauer, M. Kelley, R. Ruedy, G.L. Russell, A. Ackerman, I. Aleinov, M. Bauer, R. Bleck, V. Canuto, G. Cesana, Y. Cheng, T.L. Clune, B. Cook, C.A. Cruz, A.D. Del Genio, G.S. Elsaesser, G. Faluvegi, N.Y. Kiang, D. Kim, A.A. Lacis, A. Leboissetier, A.N. LeGrande, K.K. Lo, J. Marshall, E.E. Matthews, S. McDermid, K. Mezuman, L.T. Murray, V. Oinas, C. Orbe, C. Pérez García-Pando, J.P. Perlwitz, M.J. Puma, D. Rind, A. Romanou, D.T. Shindell, S. Sun, N. Tausnev, K. Tsigaridis, G. Tselioudis, E. Weng, J. Wu, and M.-S. Yao: CMIP6 historical simulations (1850-2014) with GISS-E2.1. J. Adv. Model. Earth Syst., in press, doi:10.1029/2019MS002034, 2020.

Miller, R.L., G.A. Schmidt, and D.T. Shindell: Forced annular variations in the 20th century Intergovernmental Panel on Climate Change Fourth Assessment Report models. J. Geophys. Res., 111, D18101, doi:10.1029/2005JD006323, 2006.

Myhre, G., D. Shindell, F.-M. Bréon, W. Collins, J. Fuglestvedt, J. Huang, D. Koch, J.-F. Lamarque, D. Lee, B. Mendoza, T. Nakajima, A. Robock, G. Stephens, T. Takemura, and H. Zhang: Anthropogenic and natural radiative forcing. In Climate Change 2013: The Physical Science Basis. Contribution of Working Group I to the Fifth Assessment Report of the Intergovernmental Panel on Climate Change. T.F. Stocker, D. Qin, G.-K. Plattner, M. Tignor, S.K. Allen, J. Doschung, A. Nauels, Y. Xia, V. Bex, and P.M. Midgley, Eds. Cambridge University Press, pp. 659-740, doi:10.1017/CBO9781107415324.018, 2013.

Platnick, S., S. A. Ackerman, M. D. King, K. Meyer, W. P. Menzel, R. E. Holz, B. A. Baum, and P. Yang: MODIS atmosphere L2 cloud product (06_L2), NASA MODIS Adaptive Processing System, Goddard Space Flight Center, 2015.

Rao, S., Klimont, Z., Smith, S.J., Van Dingenen, R., Dentener, F., Bouwman, L., Riahia, K., Amann, M., Bodirsky, B.L., van Vuuren, D.P., Reis, L.A., Calvin, K., Drouet, L., Fricko, O., Fujimori, S., Gernaat, D., Havlik, P., Harmsen, M., Hasegawa, T., Heyes, C., Hilaire, J., Luderer, G., Masui, T., Stehfest, E., Strefler, J., van der Slui, S., Tavonil, M.: Future air pollution in the Shared Socio-economic Pathways. Global Environmental Change, 42, 346-358, 2017.

Rayner, N. A., D. E. Parker, E. B. Horton, C. K. Folland, L. V. Alexander, D. P. Rowell, E. C. Kent, and A. Kaplan, Global analyses of sea surface temperature, sea ice, and night marine air temperature since the late nineteenth century, J. Geophys. Res.,108(D14), 4407, doi:10.1029/2002JD002670, 2003.

Ren, L., Yang, Y., Wang, H., Zhang, R., Wang, P., and Liao, H.: Source attribution of Arctic black carbon and sulfate aerosols and associated Arctic surface warming during 1980–2018, Atmos. Chem. Phys., 20, 9067–9085, https://doi.org/10.5194/acp-20-9067-2020, 2020.

Riahi, K.,van Vuuren, D.P., Kriegler, E., Edmonds, J., O'Neil, B.C., Fujimori, S., Bauer, N., Calvin, K., Dellink, R., Fricko, O., Lutz, W., Popp, A., Cuaresma, C.J., KC, S., Leimbach, M., Jiang, L., Kram, T., Rao, S., Emmerling, J., Ebi, K., Hasegawa, T., Havlik, P., Humpenöder, F., Da Silva, L.A:, Smith, S., Stehfest, E., Bosetti, V., Eom, J., Gernaat, D., Masui, T., Rogelj, J., Strefler, J., Drouet, L., Krey, V., Luderer, G., Harmsen, M., Takahashi, K., Baumstark, L., Doelman, J.C., Kainuma, M., Klimont, Z., Marangoni, G., Lotze-Campen, H., Obersteiner, M., Tabeau, A., Tavoni, M.: The Shared Socioeconomic Pathways and their energy, land use, and greenhouse gas emissions implications: An overview. Global Environmental Change, 42, 153-168, 2017.

Samset, B. H., Sand, M., Smith, C. J., Bauer, S. E., Forster, P. M., Fuglestvedt, J. S., Osprey, S., & Schleussner, C.-F.: Climate impacts from a removal of anthropogenic aerosol emissions. Geophysical Research Letters, 45. https://doi.org/10.1002/2017GL076079, 2018.

Sand, M., T. K. Berntsen, K. von Salzen, M. G. Flanner, J. Langner, and D. G. Victor: Response of arctic temperature to changes in emissions of short-lived climate forcers, Nat. Clim. Change, 6, 286–289, doi:10.1038/nclimate2880, 2015.

Sayer, A. M., Hsu, N. C., Lee, J., Kim, W. V., Dubovik, O., Dutcher, S. T. et al.: Validation of SOAR VIIRS over-water aerosol retrievals and context within the global satellite aerosol data record. Journal of Geophysical Research: Atmospheres, 123, 13,496–13,526, https://doi.org/10.1029/2018JD029465, 2018.

Sayer, A. M. and Knobelspiesse, K. D.: How should we aggregate data? Methods accounting for the numerical distributions, with an assessment of aerosol optical depth, Atmos. Chem. Phys., 19, 15023–15048, https://doi.org/10.5194/acp-19-15023-2019, 2019.

Schacht, J., Heinold, B., Quaas, J., Backman, J., Cherian, R., Ehrlich, A., Herber, A., Huang, W. T. K., Kondo, Y., Massling, A., Sinha, P. R., Weinzierl, B., Zanatta, M., and Tegen, I.: The importance of the representation of air pollution emissions for the modeled distribution and radiative effects of black carbon in the Arctic, Atmos. Chem. Phys., 19, 11159–11183, https://doi.org/10.5194/acp-19-11159-2019, 2019.

Schutgens, N. A. J.: Site representativity of AERONET and GAW remotely sensed aerosol optical thickness and absorbing aerosol optical thickness observations, Atmos. Chem. Phys., 20, 7473–7488, https://doi.org/10.5194/acp-20-7473-2020, 2020a.

Schutgens, N., Sayer, A. M., Heckel, A., Hsu, C., Jethva, H., de Leeuw, G., Leonard, P. J. T., Levy, R. C., Lipponen, A., Lyapustin, A., North, P., Popp, T., Poulson, C., Sawyer, V., Sogacheva, L., Thomas, G., Torres, O., Wang, Y., Kinne, S., Schulz, M., and Stier, P.: An AeroCom/AeroSat study: Intercomparison of Satellite AOD Datasets for Aerosol Model Evaluation, Atmos. Chem. Phys. Discuss., https://doi.org/10.5194/acp-2019-1193, in review, 2020b.

Semmler, T., Pithan, F., Jung, T.: Quantifying two-way influences between the Arctic and mid-latitudes through regionally increased CO2 concentrations in coupled climate simulations, *Climate Dynamics*, 54, 3307–3321, 2020.

Serreze, M.C., Francis, J.A. The Arctic Amplification Debate. Climatic Change 76, 241–264, https://doi.org/10.1007/s10584-005-9017-y, 2006.

Shindell, D. T., Lamarque, J.-F., Schulz, M., Flanner, M., Jiao, C., Chin, M., Young, P. J., Lee, Y. H., Rotstayn, L., Mahowald, N., Milly, G., Faluvegi, G., Balkanski, Y., Collins, W. J., Conley, A. J., Dalsoren, S., Easter, R., Ghan, S., Horowitz, L., Liu, X., Myhre, G.,

https://doi.org/10.5194/acp-2020-1296
Preprint. Discussion started: 7 January 2021

Nagashima, T., Naik, V., Rumbold, S. T., Skeie, R., Sudo, K., Szopa, S., Takemura, T., Voulgarakis, A., Yoon, J.-H., and Lo, F.: Radiative forcing in the ACCMIP historical and future climate simulations, Atmos. Chem. Phys., 13, 2939–2974, https://doi.org/10.5194/acp-13-2939-2013, 2013.

Shindell, D., J.C.I. Kuylenstierna, E. Vignati, R. van Dingenen, M. Amann, Z. Klimont, S.C. Anenberg, N. Muller, G. Janssens-Maenhout, F. Raes, J. Schwartz, G. Faluvegi, L. Pozzoli, K. Kupiainen, L. Höglund-Isaksson, L. Emberson, D. Streets, V. Ramanathan, K. Hicks, N.T.K. Oanh, G. Milly, M. Williams, V. Demkine, and D. Fowler, Simultaneously mitigating near-term climate change and improving human health and food security. Science, 335, 183-189, doi:10.1126/science.1210026, 2012.

Shindell, D., and G. Faluvegi,: Climate response to regional radiative forcing during the twentieth century. Nature Geosci., 2, 294-300, doi:10.1038/ngeo473, 2009.

Shindell, D.: Local and remote contributions to Arctic warming, Geophysical Research Letters – Climate, 34, L14704, https://doi.org/10.1029/2007GL030221, 2007.

Sogacheva, L., Popp, T., Sayer, A. M., Dubovik, O., Garay, M. J., Heckel, A., Hsu, N. C., Jethva, H., Kahn, R. A., Kolmonen, P., Kosmale, M., de Leeuw, G., Levy, R. C., Litvinov, P., Lyapustin, A., North, P., Torres, O., and Arola, A.: Merging regional and global aerosol optical depth records from major available satellite products, Atmos. Chem. Phys., 20, 2031–2056, https://doi.org/10.5194/acp-20-2031-2020, 2020.

Skeie, R. B., Berntsen, T., Myhre, G., Pedersen, C. A., Ström, J., Gerland, S., and Ogren, J. A.: Black carbon in the atmosphere and snow, from pre-industrial times until present, Atmos. Chem. Phys., 11, 6809–6836, https://doi.org/10.5194/acp-11-6809-2011, 2011.

Stephens, G. L., and Coauthors,: THE CLOUDSAT MISSION AND THE A-TRAIN: A New Dimension of Space-Based Observations of Clouds and Precipitation. Bull. Amer. Meteor. Soc., 83, 1771–1790, https://doi.org/10.1175/BAMS-83-12-1771, 2002.

Stohl, A., Aamaas, B., Amann, M., Baker, L. H., Bellouin, N., Berntsen, T. K., Boucher, O., Cherian, R., Collins, W., Daskalakis, N., Dusinska, M., Eckhardt, S., Fuglestvedt, J. S., Harju, M., Heyes, C., Hodnebrog, Ø., Hao, J., Im, U., Kanakidou, M., Klimont, Z., Kupiainen, K., Law, K. S., Lund, M. T., Maas, R., MacIntosh, C. R., Myhre, G., Myriokefalitakis, S., Olivié, D., Quaas, J., Quennehen, B., Raut, J.-C., Rumbold, S. T., Samset, B. H., Schulz, M., Seland, Ø., Shine, K. P., Skeie, R. B., Wang, S., Yttri, K. E., and Zhu, T.: Evaluating the climate and air quality impacts of short-lived pollutants, Atmos. Chem. Phys., 15, 10529–10566, https://doi.org/10.5194/acp-15-10529-2015, 2015.

Stuecker, M.F., Bitz, C.M., Armour, K.C., Proistosescu, C., Kang, S.M., Xie, S.-P., Kim, D., McGregor, S., Zhang, W., Zhao, S., Cai, W., Dong, Y., Jin, F.-F.: Polar amplification dominated by local forcing and feedbacks, *Nature Climate Change*, 8, 1076–1081, 2018.

Thomas, J.L., et al.: Fostering multidisciplinary research on interactions between chemistry, biology, and physics within the coupled cryosphere-atmosphere system. Elem Sci Anth, 7: 58. DOI: https://doi.org/10.1525/elementa.396, 2019.

https://doi.org/10.5194/acp-2020-1296
Preprint. Discussion started: 7 January 2021

Atmospheric Chemistry and Physics Discussions
Open Access

Tsigaridis, K., and M. Kanakidou,: Secondary organic aerosol importance in the future atmosphere. Atmos. Environ., 41, 4682-4692, doi:10.1016/j.atmosenv.2007.03.045, 2007.

Turnock, S. T., Allen, R. J., Andrews, M., Bauer, S. E., Deushi, M., Emmons, L., Good, P., Horowitz, L., John, J. G., Michou, M., Nabat, P., Naik, V., Neubauer, D., O'Connor, F. M., Olivié, D., Oshima, N., Schulz, M., Sellar, A., Shim, S., Takemura, T., Tilmes, S., Tsigaridis, K., Wu, T., and Zhang, J.: Historical and future changes in air pollutants from CMIP6 models, Atmos. Chem. Phys., 20, 14547–14579, https://doi.org/10.5194/acp-20-14547-2020, 2020.

van Marle, M. J. E., Kloster, S., Magi, B. I., Marlon, J. R., Daniau, A.-L., Field, R. D., Arneth, A., Forrest, M., Hantson, S., Kehrwald, N. M., Knorr, W., Lasslop, G., Li, F., Mangeon, S., Yue, C., Kaiser, J. W., and van der Werf, G. R.: Historic global biomass burning emissions for CMIP6 (BB4CMIP) based on merging satellite observations with proxies and fire models (1750–2015), Geosci. Model Dev., 10, 3329–3357, https://doi.org/10.5194/gmd-10-3329-2017, 2017.

Wei, J., Peng, Y., Mahmood, R., Sun, L., and Guo, J.: Intercomparison in spatial distributions and temporal trends derived from multi-source satellite aerosol products, Atmos. Chem. Phys., 19, 7183–7207, https://doi.org/10.5194/acp-19-7183-2019, 2019.

Westervelt, D. M., Horowitz, L. W., Naik, V., Golaz, J.-C., & Mauzerall, D. L.: Radiative forcing and climate response to projected 21st century aerosol decreases. Atmospheric Chemistry and Physics, 15, 12,681– 12,703. https://doi.org/10.5194/acp-15-12681-2015, 2015.

Willis, M. D., Leaitch, W. R., &Abbatt, J. P.: Processescontrolling the composition andabundance of Arctic aerosol.Reviews of Geophysics, 56, 621–671. https://doi.org/10.1029/2018RG000602, 2018.

Willmott, C. J. and K. Matsuura,: Terrestrial Air Temperature and Precipitation: Monthly and Annual Time Series (1950 - 1999), 2001. (http://climate.geog.udel.edu/~climate/html_pages/README.ghcn_ts2.html, (last access: October 26th)

https://doi.org/10.5194/acp-2020-1296
Preprint. Discussion started: 7 January 2021

Atmospheric Chemistry and Physics Discussions

Tables

Table 1. GISS-E2.1 simulations carried out in the Eclipse and CMIP6 ensembles.

Simulations	Description	No. Ensemble	Period
NINT_Cpl	No tracers- Coupled	1	1850-2014
Eclipse_AMIP	AMIP OMA	1	1995-2014
Eclipse_AMIP_NCEP	AMIP OMA – winds nudged to NCEP	1	1995-2014
Eclipse_CplHist	OMA – Coupled	3	1990-2014
Eclipse_Cpl_CLE	OMA – Coupled	3	2015-2050
Eclipse_Cpl_MFR	OMA – Coupled	3	2020-2050
CMIP6_Cpl_Hist	OMA – Coupled	1	1850-2014
CMIP6_Cpl_SSP1-2.6	OMA – Coupled	1	2015-2050
CMIP6_Cpl_SSP2-4.5	OMA – Coupled	1	2015-2050
CMIP6_Cpl_SSP3-7.0	OMA – Coupled	1	2015-2050
CMIP6_Cpl_SSP3-7.0-lowNTCF	OMA – Coupled	1	2015-2050

Table 2. Annual mean Normalised Mean Bias (*NMB:%*) and correlation coefficients (*r*) for the recent past simulations in the GISS-E2.1 model ensemble during 1995-2014 for BC, OC, SO_4^{2-} and 2008/2009-2014 for AOD550 from AERONET and satellites.

	BC		OC		SO_4^{2-}		AOD_aero		AOD_sat	
Model	*NMB*	*r*	*NMB*	*r*	*NMB*	*r*	*NMB*	*r*	*NMB*	*r*
AMAP_OnlyAtm.	-67.32	0.27	-35.46	0.54	-49.83	0.65	-33.28	-0.07	-0.48	0.00
AMAP_OnlyAtm_NCEP	-57.00	0.26	-7.80	0.56	-52.70	0.74	-41.99	0.02	-0.55	0.13
AMAP_CplHist1	-62.82	0.21	-22.85	0.51	-50.13	0.70	-47.42	0.03	-0.59	-0.00
AMAP_CplHist2	-63.49	0.29	-17.99	0.63	-48.44	0.71	-41.89	0.01	-0.55	0.1
AMAP_CplHist3	-62.70	0.27	-16.36	0.60	-49.60	0.70	-40.53	0.07	-0.53	0.11
CMIP6_Cpl_Hist	-49.90	0.26	13.14	0.69	-39.81	0.70	-39.86	0.05	-0.53	0.11

https://doi.org/10.5194/acp-2020-1296
Preprint. Discussion started: 7 January 2021

Atmospheric Chemistry and Physics Discussions
Open Access
EGU

Table 3. Annual mean biases and correlation coefficients (*r*) for the recent past simulations in the GISS-E2.1 model ensemble in 1995-2014 for surface air temperature (Tsurf) and sea surface temperature (SST) in units of °C, and precipitation (Precip), sea-ice fraction (Sea-ice), total cloud fraction (CldFrc), liquid water path (LWP), and ice water path (IWP) in units of %.

	IWP		LWP		Cld Frac		Sea-ice		SST		Precip		Tsurf	
Simulations	*r*	*NMB (%)*	*r*	*NMB (%)*	*r*	*NMB (%)*	*r*	*NMB (%)*	*r*	*MB (°C)*	*r*	*NMB (%)*	*r*	*MB (°C)*
NINT	0.53	-56.06	-0.89	70.55	-0.67	20.95	1.00	12.14	0.99	-1.96	0.88	-52.68	1.00	-0.22
AMAP_OnlyAtm.	-0.18	-58.53	-0.96	57.52	-0.81	23.78	1.00	-2.56	0.99	-1.50	0.89	-50.33	1.00	0.55
AMAP_OnlyAtm_NCEP	-0.64	-70.32	-0.91	14.19	-0.79	24.83	1.00	-2.56	0.99	-1.50	0.90	-53.19	1.00	0.35
AMAP_CplHist1	0.56	-55.38	-0.90	72.60	-0.66	21.63	1.00	11.04	0.99	-1.93	0.87	-52.63	1.00	-0.04
AMAP_CplHist2	0.44	-56.53	-0.93	68.63	-0.65	21.48	0.99	11.13	0.99	-1.92	0.84	-53.96	1.00	-0.09
AMAP_CplHist3	0.45	-55.32	-0.91	71.75	-0.66	21.79	1.00	11.88	0.99	-1.94	0.86	-52.59	1.00	-0.14
CMIP6_Cpl_Hist	0.40	-56.28	-0.91	69.18	-0.65	21.49	0.99	12.56	0.98	-1.96	0.85	-53.96	1.00	-0.17

https://doi.org/10.5194/acp-2020-1296
Preprint. Discussion started: 7 January 2021

Atmospheric Chemistry and Physics Discussions
Open Access
EGU

Table 4. TOA aerosol radiative forcings for 1990-2010 and 2030-2050 periods as calculated by the GISS-E2.1.

	SSA		Dust		NO3		SO4		OC		BC		Aerosols Anth.		Aerosols Total	
Simulations	2030-2050	1990-2010	2030-2050	1990-2010	2030-2050	1990-2010	2030-2050	1990-2010	2030-2050	1990-2010	2030-2050	1990-2010	2030-2050	1990-2010	2030-2050	1990-2010
NINT_Cpl		-0.23		0.06		-0.01		-0.33		-0.05		0.2		-0.19		-0.35
Eclipse_AMIP		-0.27		0.09		-0.02		-0.39		-0.06		0.2		-0.27		-0.46
Eclipse_AMIP_NCEP		-0.23		0.08		-0.04		-0.39		-0.08		0.19		-0.32		-0.47
Eclipse_CplHist_3xEns		-0.22		0.12		-0.03		-0.38		-0.05		0.23		-0.22		-0.32
Eclipse_CplCLE_3xEns	-0.24		0.09		-0.07		-0.27		-0.07		0.17		-0.24		-0.39	
Eclipse_CplMFR_3xEns	-0.25		0.09		-0.04		-0.22		-0.07		0.09		-0.23		-0.39	
CMIP6_Cpl_Hist		-0.21		0.12		-0.04		-0.4		-0.06		0.23		-0.26		-0.35
CMIP6_Cpl_SSP126	-0.24		0.09		-0.1		-0.22		-0.07		0.13		-0.26		-0.4	
CMIP6_Cpl_SSP245	-0.23		0.09		-0.09		-0.29		-0.08		0.19		-0.27		-0.41	
CMIP6_Cpl_SSP370	-0.23		0.09		-0.06		-0.34		-0.09		0.28		-0.21		-0.35	
CMIP6_Cpl_SSP370-lowNTCF	-0.23		0.09		-0.09		-0.28		-0.07		0.2		-0.24		-0.38	

https://doi.org/10.5194/acp-2020-1296
Preprint. Discussion started: 7 January 2021

Atmospheric Chemistry and Physics
Discussions

Figures

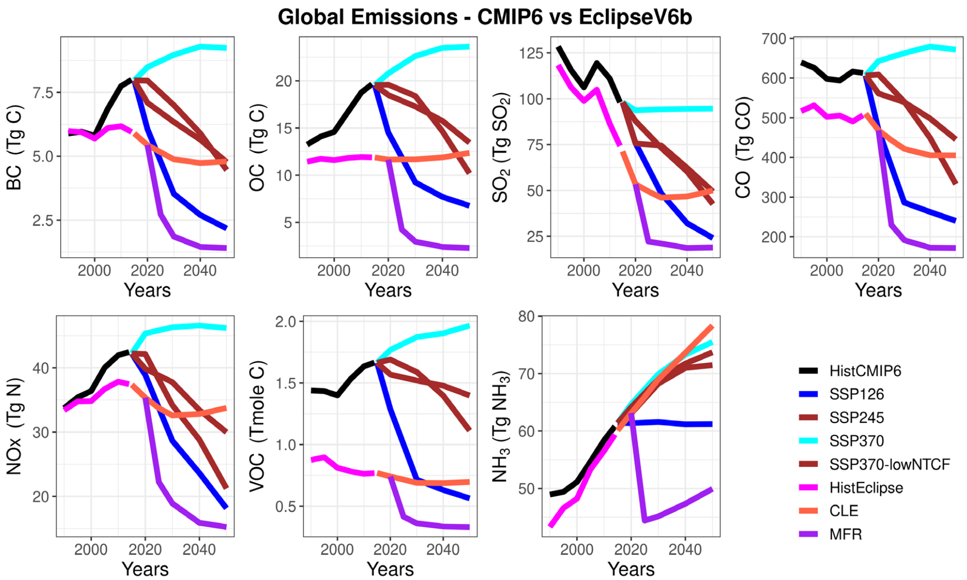

Figure 1. Global recent past and future CMIP6 and Eclipse V6b anthropogenic emissions for different pollutants and scenarios.

https://doi.org/10.5194/acp-2020-1296
Preprint. Discussion started: 7 January 2021

Atmospheric Chemistry and Physics
Discussions

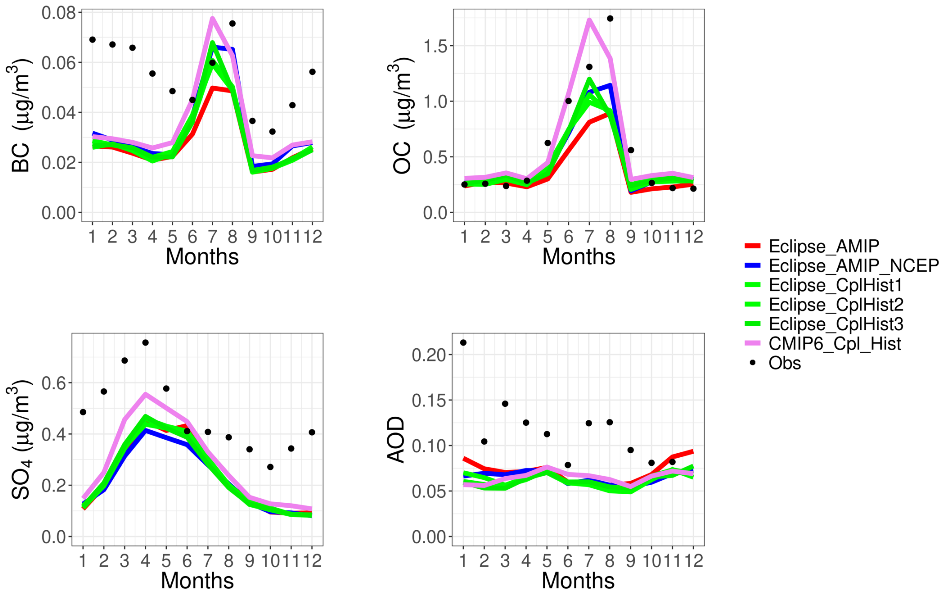

Figure 2. Observed and simulated Arctic climatological (1995-2014) monthly BC, OC, SO_4^{2-}, and AERONET AOD at 550nm (2008/09-14).

https://doi.org/10.5194/acp-2020-1296
Preprint. Discussion started: 7 January 2021

Atmospheric Chemistry and Physics
Open Access
Discussions

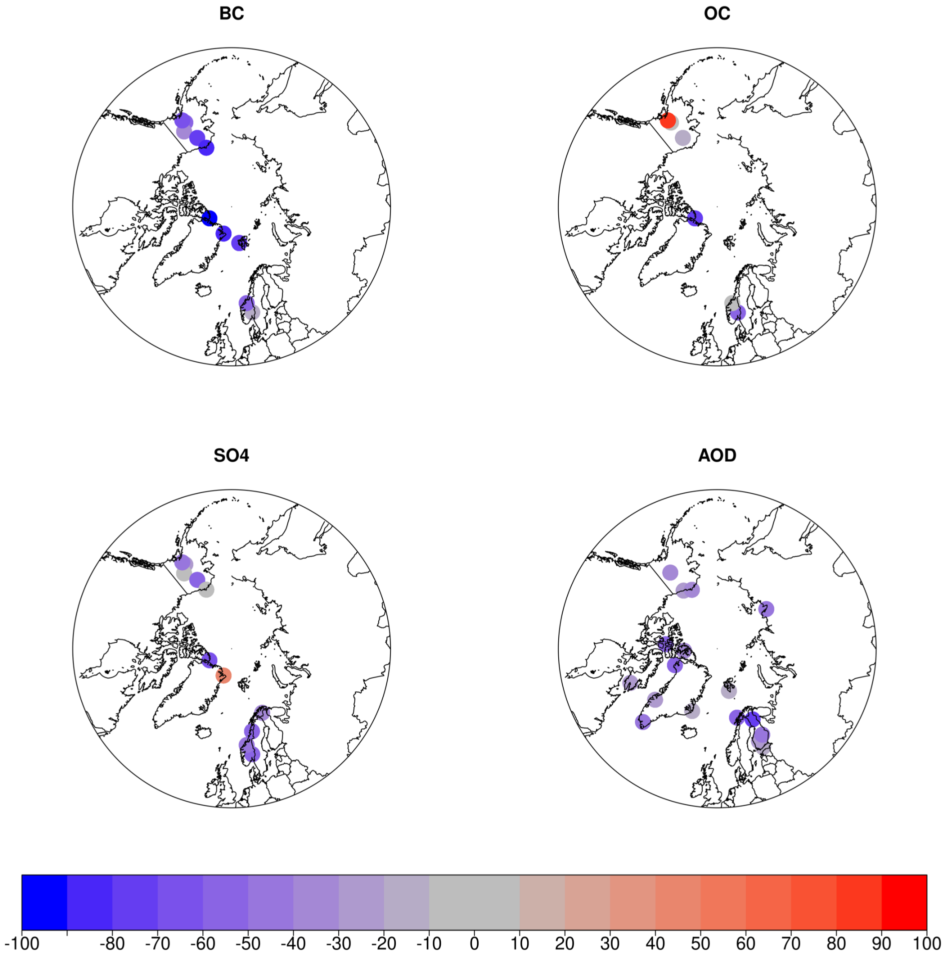

Figure 3. Spatial distribution of normalized mean bias (*NMB*, in %) for climatological mean (1995-2014) BC, OC, SO_4^{2-} and AOD at monitoring stations, calculated as the mean of all recent past simulations.

https://doi.org/10.5194/acp-2020-1296
Preprint. Discussion started: 7 January 2021

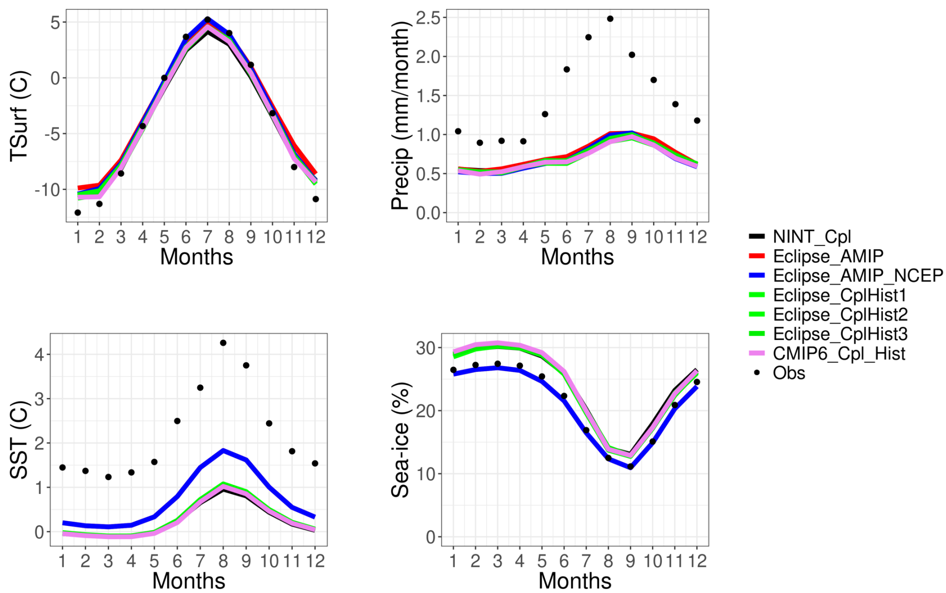

Figure 4. Observed and simulated Arctic climatological (1995-2014) surface air temperature, precipitation, sea surface temperature, and sea-ice. Obs denote UDel dataset for surface air temperature and precipitation, and HADISST for sea surface temperature and sea-ice extent. Note that the two AMIP runs (blue and red lines) for the SST and sea-ice are on top of each other as they use that data to run, as input.

https://doi.org/10.5194/acp-2020-1296
Preprint. Discussion started: 7 January 2021

Atmospheric Chemistry and Physics
Discussions

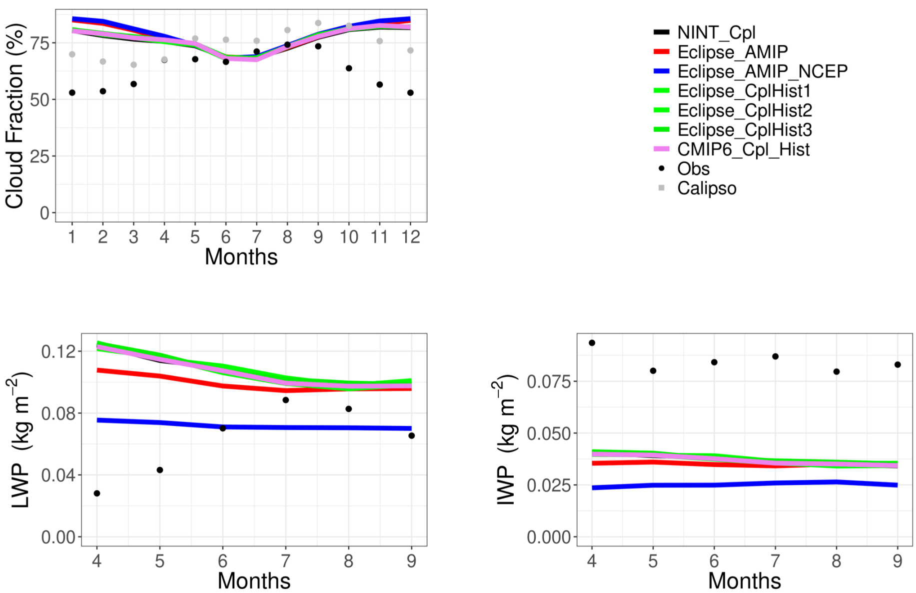

Figure 5. Observed and simulated Arctic climatological total cloud fraction (1995-2014 mean), liquid water path (2007-2014 mean), and ice water path (2007-2014 mean). Obs denote Clara-A2 for the cloud fractions and CloudSat for the LWP and IWP.

https://doi.org/10.5194/acp-2020-1296
Preprint. Discussion started: 7 January 2021

Atmospheric Chemistry and Physics Discussions
Open Access
EGU

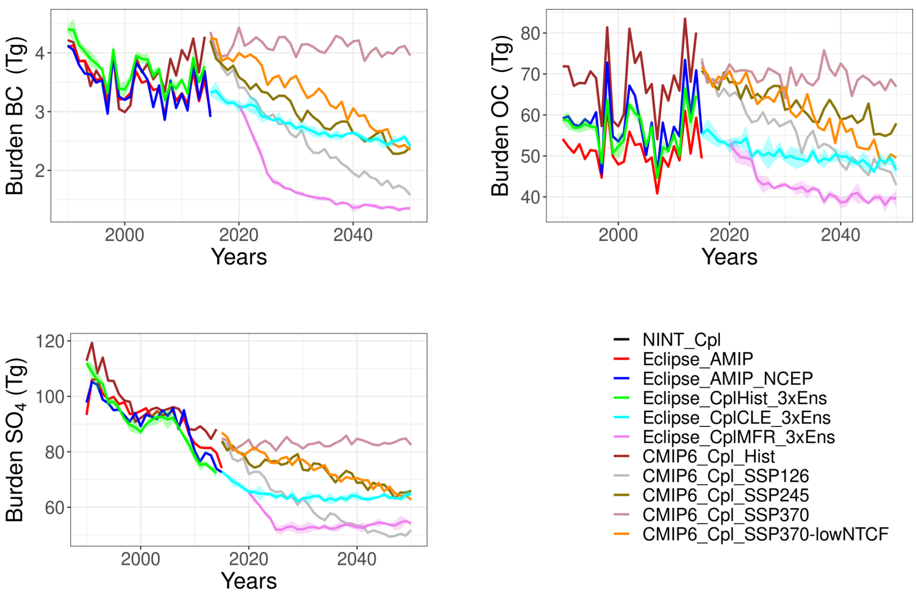

Figure 6. Arctic BC, OC and SO_4^{2-} burdens in 1990-2050 as calculated by the GISS-E2.1 ensemble.

https://doi.org/10.5194/acp-2020-1296
Preprint. Discussion started: 7 January 2021

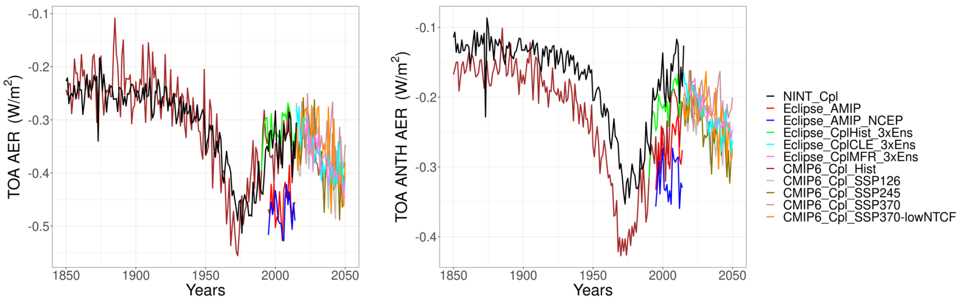

Figure 7. Arctic TOA aerosol radiative forcing from anthropogenic and natural aerosols (BC+OC+SO_4^{2-}+NO_3^-+Dust+SSA), and only anthropogenic aerosols (BC+OC+SO_4^{2-}+NO_3^-) in 1850-2050 as calculated by the full GISS-E2.1 ensemble.

https://doi.org/10.5194/acp-2020-1296
Preprint. Discussion started: 7 January 2021

Atmospheric Chemistry and Physics
Open Access
Discussions
EGU

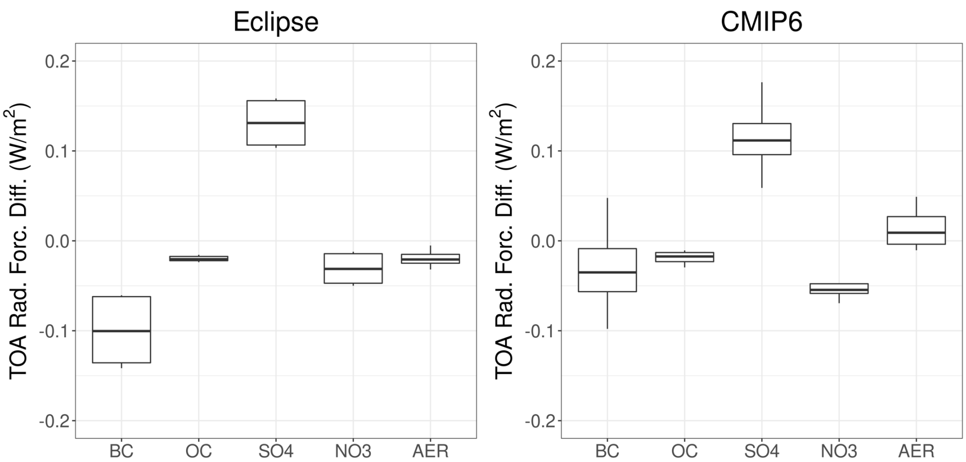

Figure 8. Box-Whisker plot showing the differences between 1990-2010 mean and 2030-2050 mean TOA radiative forcing for the anthropogenic aerosol components (BC, OC, SO_4^{2-} and NO_3^-) and their sum (AER) in the Eclipse (left panel) and the CMIP6 (right panel) ensembles. The boxes show the median, the 25th and 75th percentiles. The upper whisker is located at the *smaller* of the maximum value and Q_3 + 1.5 IQR, whereas the lower whisker is located at the *larger* of the smallest x value and Q_1 – 1.5 IQR, where IQR (interquartile range) is the box height (75th percentile - 25th percentile).

https://doi.org/10.5194/acp-2020-1296
Preprint. Discussion started: 7 January 2021

Atmospheric Chemistry and Physics
Discussions

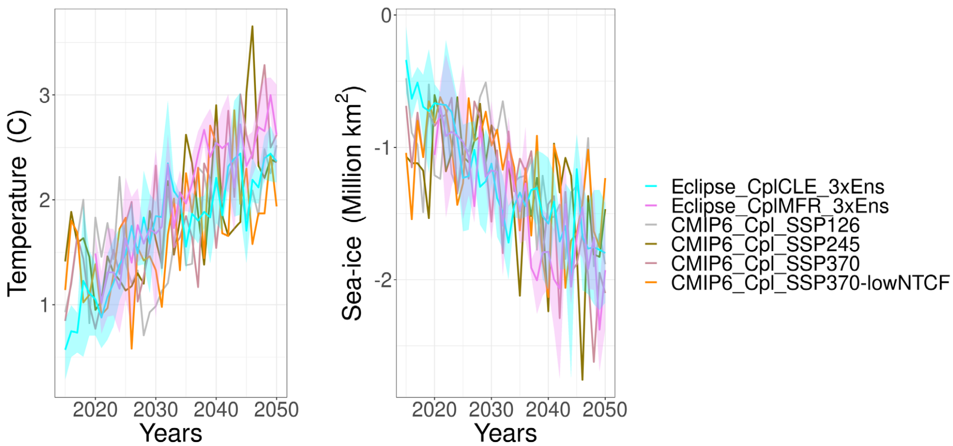

Figure 9. Arctic annual mean surface air temperature and sea-ice extent anomalies in 2015-2050 based on the 1990-2010 mean as calculated by the GISS-E2.1 ensemble.

https://doi.org/10.5194/acp-2020-1296
Preprint. Discussion started: 7 January 2021

Atmospheric Chemistry and Physics
Discussions

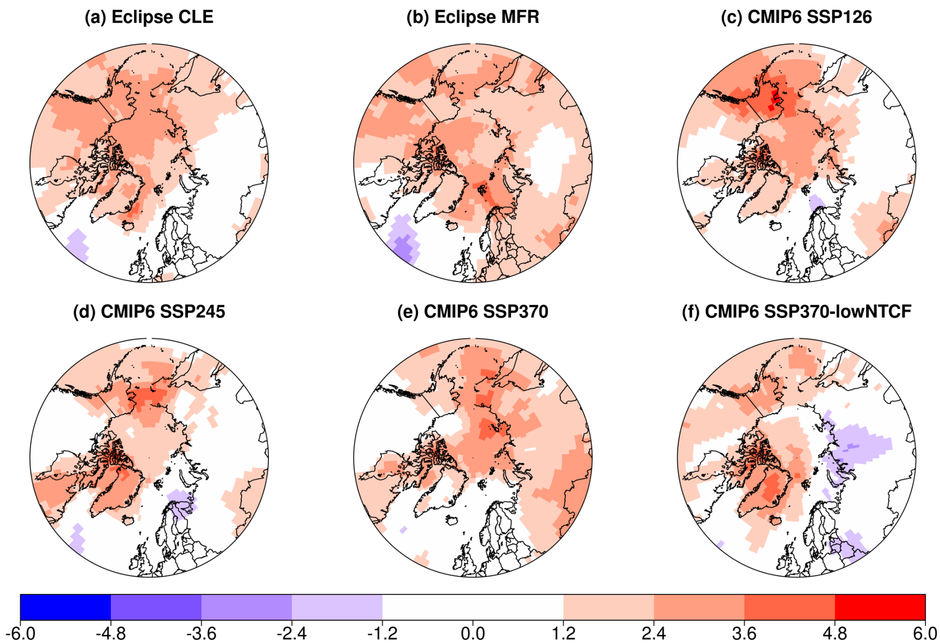

Figure 10. Spatial distribution of the annual mean Arctic surface air temperature (°C) changes between the 1990-2010 mean and the 2030-2050 mean as calculated by the GISS-E2.1 ensemble.

https://doi.org/10.5194/acp-2020-1296
Preprint. Discussion started: 7 January 2021

Atmospheric Chemistry and Physics
Discussions

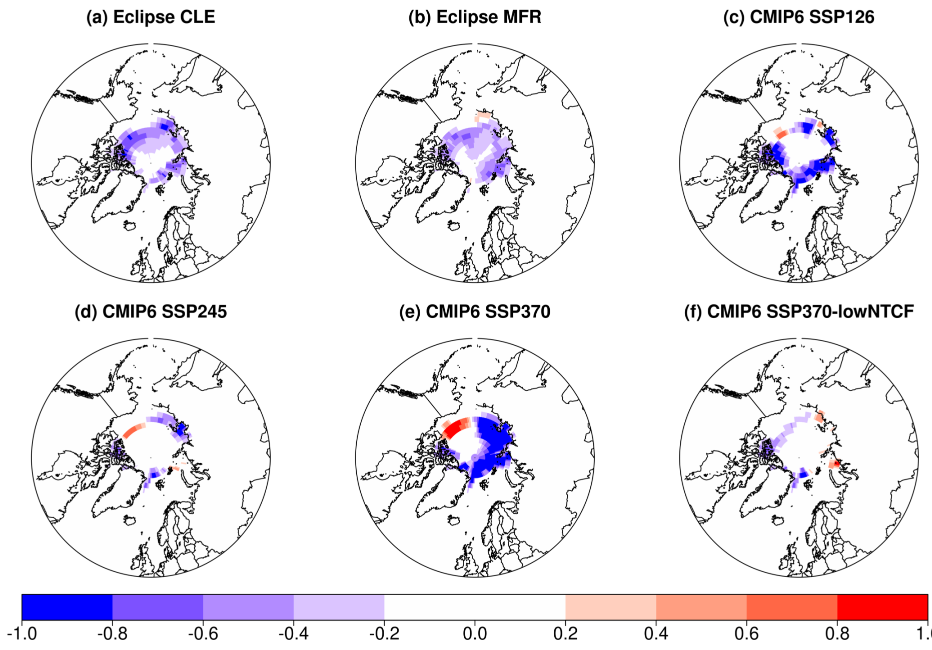

Figure 11. Spatial distribution of the September Arctic sea-ice fraction change between the 1990-2010 mean and the 2030-2050 mean as calculated by the GISS-E2.1 ensemble.